Provided for non-commercial research and education use.
Not for reproduction, distribution or commercial use.

Volume 56 Number 1 January 2009 ISSN 0967-0637

ELSEVIER

DEEP-SEA RESEARCH

PART I

Editor:
Michael P. Bacon
Woods Hole, MA, USA

Oceanographic Research Papers

V.V. IVANOV, I.V. POLYAKOV, I.A. DMITRENKO, E. HANSEN, I.A. REPINA, S.A. KIRILLOV, C. MAURITZEN, H. SIMMONS and L.A. TIMOKHOV — 1 Seasonal variability in Atlantic Water off Spitsbergen

F. D'OVIDIO, J. ISERN-FONTANET, C. LÓPEZ, E. HERNÁNDEZ-GARCÍA and E. GARCÍA-LADONA — 15 Comparison between Eulerian diagnostics and finite-size Lyapunov exponents computed from altimetry in the Algerian basin

D. KADKO and K. AAGAARD — 32 Glimpses of Arctic Ocean shelf–basin interaction from submarine-borne radium sampling

C.S. MEINEN, D.S. LUTHER and M.O. BARINGER — 41 Structure, transport and potential vorticity of the Gulf Stream at 68°W: Revisiting older data sets with new techniques

K.-I. CHANG, K. KIM, Y.-B. KIM, W.J. TEAGUE, J. CHUL LEE and J.-H. LEE — 61 Deep flow and transport through the Ulleung Interplain Gap in the Southwestern East/Japan Sea

C.C.S. HANNIDES, M.R. LANDRY, C.R. BENITEZ-NELSON, R.M. STYLES, J.P. MONTOYA and D.M. KARL — 73 Export stoichiometry and migrant-mediated flux of phosphorus in the North Pacific Subtropical Gyre

I. WILKE, H. MEGGERS and T. BICKERT — 89 Depth habitats and seasonal distributions of recent planktic foraminifers in the Canary Islands region (29°N) based on oxygen isotopes

D. STORZ, H. SCHULZ, J.J. WANIEK, D.E. SCHULZ-BULL and M. KUČERA — 107 Seasonal and interannual variability of the planktic foraminiferal flux in the vicinity of the Azores Current

L. IGNACIO VILCHIS, L.T. BALLANCE and W. WATSON — 125 Temporal variability of neustonic ichthyoplankton assemblages of the eastern Pacific warm pool: Can community structure be linked to climate variability?

www.elsevier.com/locate/dsri

This article appeared in a journal published by Elsevier. The attached copy is furnished to the author for internal non-commercial research and education use, including for instruction at the authors institution and sharing with colleagues.

Other uses, including reproduction and distribution, or selling or licensing copies, or posting to personal, institutional or third party websites are prohibited.

In most cases authors are permitted to post their version of the article (e.g. in Word or Tex form) to their personal website or institutional repository. Authors requiring further information regarding Elsevier's archiving and manuscript policies are encouraged to visit:

http://www.elsevier.com/copyright

Author's personal copy

Deep-Sea Research I 56 (2009) 41–60

Contents lists available at ScienceDirect

Deep-Sea Research I

journal homepage: www.elsevier.com/locate/dsri

Structure, transport and potential vorticity of the Gulf Stream at 68°W: Revisiting older data sets with new techniques

Christopher S. Meinen [a,*], Douglas S. Luther [b,1], Molly O. Baringer [a,2]

[a] Atlantic Oceanographic and Meteorological Laboratory, Miami, FL, USA
[b] School of Ocean and Earth Science and Technology, University of Hawaii at Manoa, Honolulu, HI, USA

ARTICLE INFO

Article history:
Received 14 February 2008
Received in revised form
23 July 2008
Accepted 29 July 2008
Available online 3 August 2008

Keywords:
Gulf Stream
Stream coordinates
Inverted echo sounder
IES
PIES
Western boundary current

ABSTRACT

The stream-coordinates mean structure of the Gulf Stream at 68°W is derived using new methods for both defining stream coordinates and interpreting bottom pressure and inverted echo sounder travel times collected during the extensive Synoptic Ocean Prediction experiment. These new analyses provide pictures of the vertical structure of Gulf Stream flows that are demonstrably dynamically consistent with the density field at all depths, in contrast to previous work that relies on simple vertical interpolations to fill gaps between sparse current meter measurements. This new view of the Gulf Stream suggests a slightly higher total mean transport, with the increases coming from both baroclinic and barotropic components, and slightly stronger recirculation cells, particularly on the southern side. The recirculation of the Gulf Stream appears to have a weak baroclinic component, perhaps 10% of the total. A significant advantage of the methodology is the ability to obtain sensible vertical and horizontal gradients of currents and density so that the vertical and cross-stream structures of the components of the mean potential vorticity can be clearly imaged. One new feature from this calculation is that the along-stream gradient of the cross-stream velocity, a term that is often ignored in potential vorticity analyses, is non-negligible (though small) and is asymmetric about the current axis. Both the derived structure and implied dynamics of the circulation can be significantly altered by small changes to the method of calculating daily stream coordinates, e.g., by carefully filtering out observations in rings or not. Arrays of pressure-equipped inverted echo sounders provide the opportunity (at reasonable cost) for properly defining the stream coordinates of energetic jets such as the Gulf Stream.

Published by Elsevier Ltd.

1. Introduction

Although the Gulf Stream is quite probably the most extensively observed current in the world, there still does not exist a dynamically consistent picture of the complete vertical structure of its mean currents nor its water properties (the emphasis here is on the word 'mean', since consistent snapshots of the current structures and water properties have been produced). Such information is much more than a curiosity because the search for small variations in the structure of the ocean due to climate change requires an accurate baseline of observations of mean transports of mass and water properties. As well, investigations of the nuances of the dynamics of the Gulf Stream, for their intrinsic value and for numerical model validation, require dynamically consistent observations of the vertical and horizontal Gulf Stream structure.

* Corresponding author. Tel.: +1 305 361 4355; fax: +1 305 361 4412.
E-mail addresses: Christopher.Meinen@noaa.gov (C.S. Meinen), dluther@hawaii.edu (D.S. Luther), Molly.Baringer@noaa.gov (M.O. Baringer).
[1] Tel.: +1 808 956 5875.
[2] Tel.: +1 305 361 4345.

0967-0637/$ - see front matter Published by Elsevier Ltd.
doi:10.1016/j.dsr.2008.07.010

Author's personal copy

Along with the many studies of the Gulf Stream over the past decades there has been a steady march of improved hypotheses elucidating the dynamics and energetics of the Gulf Stream, and concurrently there has been a steady improvement of instrumentation and the development of more powerful techniques for analyzing observations. The availability of newer, and arguably 'better', techniques for the analysis of observations suggests that the time is right to revisit well studied regions such as the Gulf Stream at 68°W to see what new knowledge can be uncovered from prior observations.

The Synoptic Ocean Prediction (SYNOP) experiment was one of the largest studies of the Gulf Stream system, with moored arrays and Lagrangian float measurements spanning the area from Cape Hatteras out to 55°W during 1988–1990 (e.g. Pickart and Watts, 1990a; Johns et al., 1995; Shay et al., 1995, Watts et al., 1995; Bower and Hogg, 1996). There were three primary arrays of moorings during the SYNOP experiment: an array just downstream of Cape Hatteras called the Inlet Array, the main array at 68°W called the Central Array (Fig. 1a), and a large array at 55°W called the Eastern Array. The experiment involved a host of institutions including the Universities of Miami, North Carolina, and Rhode Island, as well as the Massachusetts Institute of Technology, the Naval Research Laboratory, the Scripps Institution of Oceanography, and the Woods Hole Oceanographic Institution. There have been many publications based on this project; however of particular relevance to this paper was a study of the stream-coordinates structure of the Gulf Stream at the Central Array (Johns et al., 1995, hereafter JSBW95).

In the JSBW95 study only the current meter data set was used in the calculation of the stream-coordinates mean temperature and velocity, with the inverted echo sounder data being used to provide only the pressure of the 12 °C isotherm (see Fig. 1a for instrument locations used in the Central Array). To obtain complete vertical sections, the JSBW95 study employed interpolation and extrapolation over large vertical distances from the four instrument levels on each mooring. Subsequent studies around the globe, including some by the lead author of the JSBW95 article (e.g. Johns et al., 2005), have clearly demonstrated the advantages in determining the structure and transport of a strong ocean flow using a dynamically consistent, geostrophic style of velocity estimation rather than the point current meter moorings of the type used in JSBW95. Also in the past 12 years it has been shown that the combination of inverted echo sounder, bottom pressure, and hydrographic data can produce a more complete estimate of the vertical structure of temperature, salinity, and absolute geostrophic velocity than is possible from a small number of instruments distributed on a mooring (e.g. Meinen and Watts, 2000; Watts et al., 2001a). And finally, it is now known that the daily determination of stream coordinates can be improved by changing one of the definitions used in the JSBW95 study (Meinen and Luther, 2003).

The present paper details some results of a study of the stream-coordinates mean structure and transport of the Gulf Stream using new techniques of both stream-coordinates estimation and water property profile derivation from inverted echo sounder, pressure and hydrographic data. This work utilizes the SYNOP inverted echo sounder data to a far greater extent than occurred during the original analyses, in particular providing new estimates of the components of the potential vorticity of the flow, including a term that is often neglected but is not negligible.

2. Data

The Inverted Echo Sounder (IES) is an instrument that has been around for 30+ years (e.g. Rossby, 1969; Watts and Rossby, 1977), so a brief discussion of the instrument and its measurement is all that is provided here, with the details left to other publications (e.g. Meinen and Watts, 2000; Watts et al., 2001a). The IES is a small package about 0.6 m in height that is moored approximately one meter off the ocean bottom. The basic IES essentially consists of a 10 kHz (or 12 kHz in newer models) transmitter/receiver and a high precision clock. The IES sends out sound pulses and measures the time required for a sound pulse to travel up to the sea-surface, reflect and return to the instrument at the ocean bottom. Variations of the speed of sound in seawater, caused by changes in temperature and salinity, result in changes in the measured round-trip acoustic travel times. In the initial analyses of the SYNOP experiment the travel time variations were used solely to determine the main thermocline vertical displacements. With techniques developed more recently, the same travel time variations, when combined with hydrographic data, provide estimates of a much wider variety of information including the vertical profiles of properties and their integrals in the water column above the IES (Meinen and Watts, 2000; Watts et al., 2001a).

In the SYNOP experiment Central Array, 24 IES were deployed with nominal spacings of 40–60 km during two consecutive year-long settings (Fig. 1a). As shown in Tracey et al. (1997), the SYNOP IES travel times were originally calibrated into the quantity $Z_{12}{}^*$, which is essentially a measure of the vertically integrated temperature between 250 and 750 dbar.[3] The $Z_{12}{}^*$ values were subsequently mapped using optimal interpolation (OI) onto a regular 20 km grid (Fig. 1b). The Tracey et al. OI maps of $Z_{12}{}^*$ are employed in the present study, since the calibration accomplished by Tracey et al. (1997) is the best that can be achieved with the data collected.

Some IES packages are equipped with additional sensors; in the case of the SYNOP instruments the central core of 12 instruments was equipped with high precision bottom pressure sensors (Fig. 1a). The resolution of these sensors is better than 0.001 dbar (Watts and Kontoyiannis, 1990), with residual sensor drifts after drift correction of no more than 0.015 dbar per year (Watts et al., 2001b).

[3] Subsequent analyses of IES data have generally been calibrated into travel time at a fixed pressure surface or dynamic height anomaly at a particular level. However, because the calibration profiles collected in the SYNOP experiment were made with expendable bathythermographs rather than CTDs these more modern techniques are not possible with the SYNOP IES records.

Author's personal copy

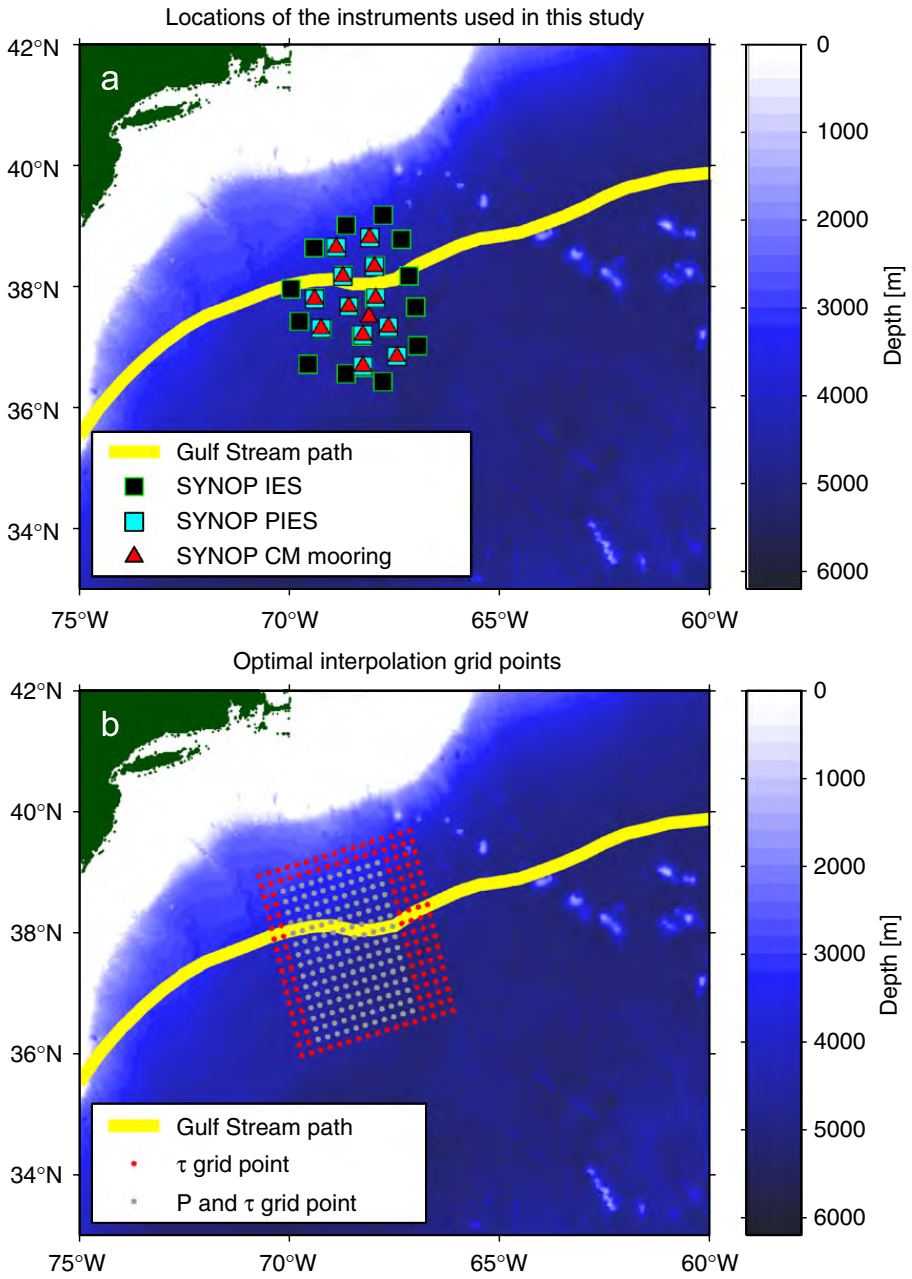

Fig. 1. (a) Map of the inverted echo sounders (IES), pressure-equipped inverted echo sounders (PIES) and current meter (CM) moorings from the SYNOP experiment during 1988–1990. The 8-year mean position of the Gulf Stream SST front (Lee and Cornillon, 1996) is shown to illustrate the position of the array relative to the current. Bottom topography from Smith and Sandwell (1997) is also shown. (b) Map showing the grid points for optimal interpolation mapping of the IES acoustic travel time, τ, and the PIES pressure data, P (Watts et al., 1995, 2001b; Tracey et al., 1997).

Watts et al. (2001b) mapped the bottom pressure data from the PIES using OI onto a 20 km grid that was slightly smaller than the $Z_{12}{}^*$ maps (Fig. 1b) because the outer ring of IES instruments did not include pressure sensors. The Watts et al. OI maps of pressure are employed in the present study.

Modern analysis of IES data requires hydrographic data from the region of study, although the data do not necessarily need to be contemporaneous. For this study, a data set of 333 conductivity-temperature-depth (CTD) profiles in the area was available from the Anatomy of a Meander project (e.g. Hummon and Rossby, 1998), several transects and ring studies by the University of Rhode Island (e.g. Johns et al., 1989) and the Woods Hole Oceanographic Institution (e.g. Joyce, 1984; Joyce et al., 1986), and from the Hydrobase data set (Lozier et al., 1995). All CTD profiles were required to reach at least 1000 dbar and have a near-surface observation within the upper 50 dbar. For profiles that lacked a surface value, the nearest-to-surface value was copied to the surface assuming a well-mixed layer above 50 dbar.

Finally, the last data sets used herein are the current meter velocity and pressure data from 13 tall current meter moorings (see Fig. 1a for locations) that were collocated with the PIES (except for one mooring set only during the second year of the experiment without a PIES

Author's personal copy

near its base). Each of the current meter moorings had instruments at nominal depths of 400, 700, 1000, and 3500 dbar (see JSBW95 for a complete discussion of the current meter data set). Shallower instrument levels included temperature and pressure measurements as well as current meter velocity measurements, while the deepest level had temperature but not pressure. The individual current meter moorings exhibited pressure deflections (blow-over) with root-mean-squared values of 75–150 m, and a maximum observed deflection of approximately 600 dbar. The current meter mooring data are used herein only to illustrate that the combination of PIES measured travel time and pressure is capable of reproducing the observed current meter signals well.

All time-series data used in creating the OI maps utilized herein were smoothed with a second order Butterworth low-pass filter with a 40-h cutoff passed both forward and backward to avoid phase shifts (Tracey et al., 1997; Watts et al., 2001b). The resulting data were then sub-sampled to once per day (noon GMT). For the bottom pressure records, Watts et al. (2001b) removed the tides using a response-analysis technique and the records were de-drifted prior to the low-pass filtering.

3. Methods

The earliest use of the IES travel time measurements was as a full-water-column calorimeter and estimator of thermocline depth (Rossby, 1969). Watts and Rossby (1977) interpreted travel times as dynamic heights and made geostrophic vertical shear comparisons with current meter and float measurements. By the late 1980s and early 1990s the IES travel times were routinely being calibrated into an estimate of the depth of the main thermocline (e.g. Watts et al., 1995), and there were some early attempts during this period to try to extract further information from the IES data using theoretical dynamical modes or the parallel isotherm assumption (e.g. Pickart and Watts, 1990b; Kim and Watts, 1994; He et al., 1998). Characteristic relationships between simulated travel time and thermocline depth/pressure were defined using hydrographic data from the region that was either coincident in time or historical (Fig. 2). By the late 1990s, after the first analyses of the SYNOP data had been completed, it was recognized that this combination of hydrography and travel time could do more than just estimate the structure of the main thermocline. Due to the high vertical coherence of the low frequency ocean variability, the IES-hydrography combination for a chosen region can also estimate the full-water-column profile of temperature, salinity, and density and it can do so empirically without any theoretical assumptions (Meinen and Watts, 2000; Watts et al., 2001a). The gravest empirical mode, or GEM, technique produces look-up tables of various water properties, including temperature, salinity, and density, as a function of pressure and an integral quantity such as round-trip acoustic travel time (Fig. 3, left panels). Mathematically any given vertical integral travel time value, which is essentially a heat content integration, could result from an infinite variety of different temperature profiles, however empirical analysis of regional hydrographic data indicates that the ocean generally associates a single type of profile with each particular integrated value within a remarkably small standard deviation. More importantly, one key feature of the GEM technique is that by comparing the original hydrographic data to the smoothed GEM look-up tables it is possible to define a data-based error bar for the GEM estimates (Fig. 3, central panels). In the SYNOP region the signal-to-noise ratios through the main thermocline depth-range (200–1200 dbar) exceed 10–20, while below the main thermocline the signal-to-noise ratios are 5–10 for all but the deepest few hundred dbar where it drops to near 1 as the signals become extremely small in comparison to the upper water column and the variations

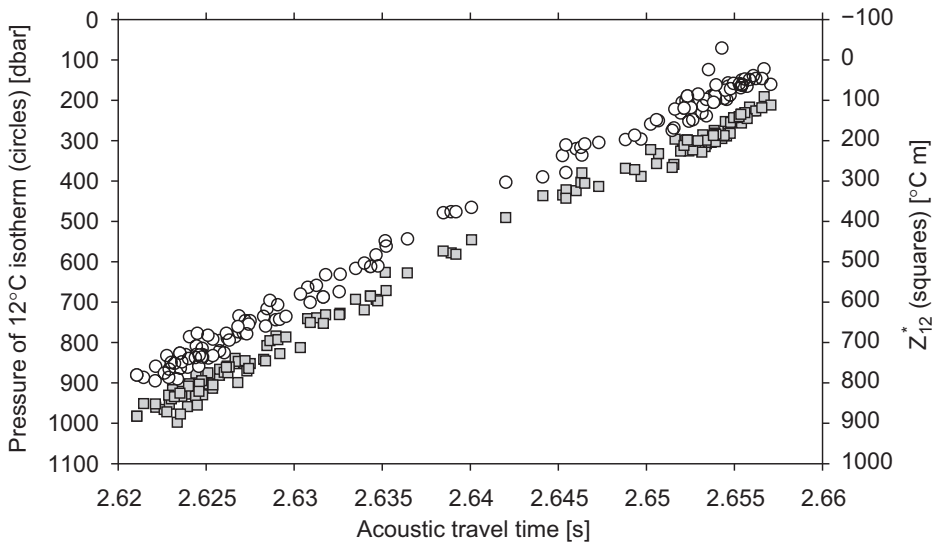

Fig. 2. Illustration of 'traditional' methods of analyzing IES acoustic travel time measurements. Hydrographic data from 333 CTD profiles was used to simulate travel time measurements by integrating sound speeds calculated from the empirical equation (Del Grosso, 1974; Meinen and Watts, 1997). The resulting simulated travel time is plotted versus the observed pressure of the 12 °C isotherm (circles) and against the value of $Z_{12}{}^*$ determined from the CTD profile (squares).

Author's personal copy

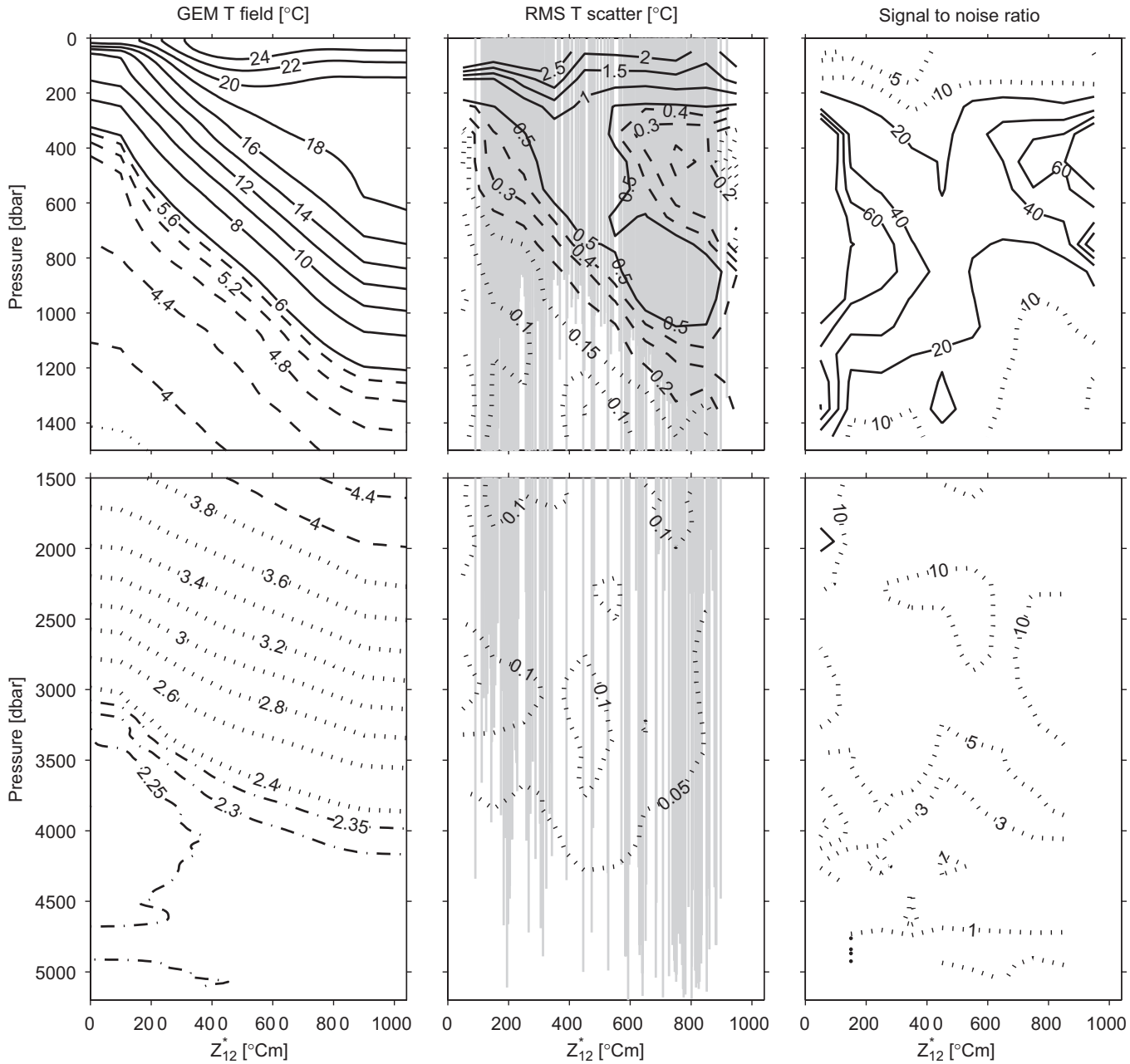

Fig. 3. Left panels: Gravest Empirical Mode (GEM) look-up table of temperature. Here the vertically-integrated temperature quantity Z_{12}^* has been used as the abscissa rather than simulated acoustic travel time because the SYNOP IES travel times were calibrated into Z_{12}^* by the original researchers at the University of Rhode Island (Watts et al., 1995; Tracey et al., 1997). Center panels: Hydrographic scatter (RMS differences) around the GEM look-up values in absolute units. Vertical gray lines indicate the original hydrographic observations. Right panels: Signal-to-noise ratio determined as the RMS differences divided into the peak-to-peak signal for each level.

are less well correlated with the thermocline variations (Fig. 3, right panels). In the surface layer the signal-to-noise ratios also drop to around 5–10, principally because of seasonal effects on the upper water column. Signal-to-noise ratios for the salinity and density (not shown) are roughly equal to those for temperature in Fig. 3. It is possible to correct for the seasonal effects in the near-surface layers by using a seasonal GEM field (Watts et al., 2001a), however these seasonal effects have large spatial scales and as such have little impact on mesoscale analyses. No seasonal GEM was applied herein.

The application in this paper of the GEM technique to the SYNOP IES travel times differs somewhat from previous applications of the GEM method. Because the SYNOP investigators calibrated their IES travel times into Z_{12}^* (using a linear relationship with travel time, see Fig. 2) prior to the OI mapping (Tracey et al., 1997), the GEM look-up tables derived herein use Z_{12}^* as the abscissa for sorting the hydrographic data into the look-up table (Fig. 3). The relationship between Z_{12}^* and travel time is sufficiently tight (see Fig. 2) that this potential source of error is negligible compared to the scatter about the GEM

Author's personal copy

field. Previous applications of the GEM technique also have involved using the IES time series at each site to extract time series of profiles of temperature, salinity, and density from the respective GEM look-up tables. For this study, rather than restrict this calculation to only the IES sites, the field of OI-gridded $Z_{12}{}^*$ (Fig. 1b) was coupled with the GEM look-up tables of temperature, salinity, and density to produce time series of profiles at each OI grid point. The result is four-dimensional grids of temperature, salinity, and density over the full-water-column with 10 dbar vertical resolution, 20 km horizontal resolution, and 1 day temporal resolution. These resolutions are generally only available using numerical model output, however in this case these grids are purely based on actual oceanic observations coupled with some basic mathematical techniques (splines for building the GEM look-up tables, OI to build the maps). Note, of course, that like all applications of OI mapping the grid points themselves do not represent independent data points, which are restricted to the original time series upon which the map is built. Neither does the vertical resolution achieved by the GEM method imply independent data every 10 dbar; nor does the 1 day temporal resolution imply independent data every day (after 40-h low-pass filtering).

Because it is possible to estimate a density profile utilizing the GEM technique, it is possible to vertically integrate this profile in order to get a dynamic height anomaly profile as well, and by differencing neighboring dynamic height profiles it is possible to calculate geostrophic velocity relative to an assumed level of no motion. Recall that we are using here the OI maps of $Z_{12}{}^*$ produced by Tracey et al. (1997); by rearranging the geostrophic balance equations we were able to calculate profiles of the horizontal gradients of the dynamic height at each OI grid point thereby yielding profiles of geostrophic relative velocity at each OI grid point shown in Fig. 1b; the zonal (U_{rel}) and meridional (V_{rel}) geostrophic relative velocity are given by

$$U_{\mathrm{rel}} = \frac{-1}{f}\frac{\delta \Delta D}{\delta y} = \frac{-1}{f}\left(\frac{\delta \Delta D}{\delta Z_{12}^*}\frac{\delta Z_{12}^*}{\delta y}\right) \quad \text{and}$$

$$V_{\mathrm{rel}} = \frac{1}{f}\frac{\delta \Delta D}{\delta x} = \frac{1}{f}\left(\frac{\delta \Delta D}{\delta Z_{12}^*}\frac{\delta Z_{12}^*}{\delta x}\right)$$

where ΔD is the dynamic height anomaly, f is the Coriolis parameter, x is the east–west distance and y is the north–south distance. The values of $\delta\Delta D/\delta Z_{12}{}^*$ are determined by taking the derivatives of splines fit to the vertically integrated density GEM field, while the values of $\delta Z_{12}{}^*/\delta x$ and $\delta Z_{12}{}^*/\delta y$ are determined by taking the gradients of splines fit to the OI maps of $Z_{12}{}^*$ produced by Tracey et al. (1997). The result is a four-dimensional grid of relative velocity at the same resolution as the temperature, salinity, and density fields. The level of no motion used for this calculation was 3500 dbar.

As noted previously, the bottom pressure measurements of the PIES cover most of the same area as the IES travel time measurements (Fig. 1). Horizontal gradients of the leveled OI maps of bottom pressure produced by Watts et al. (2001b) yield estimates of the near-bottom velocity throughout the domain covered by the bottom pressure OI maps (leveling incorporated the velocities measured by the 3500 m current meters and assumes the time-mean near-bottom velocity field was in geostrophic balance). The velocities determined as gradients of the time-varying OI pressure fields can then provide an absolute velocity reference for the four-dimensional grids of relative velocity derived from the IES measurements, yielding four-dimensional grids (within the slightly smaller mapped pressure domain, see Fig. 1) of absolute geostrophic velocity to go with the relative velocity, temperature, salinity, and density grids.

Previous applications of the GEM technique have demonstrated that the temperature, velocity and transport estimates that result from the combination of the GEM look-up tables and IES travel time records agree well with independent data such as that from moored current meters and temperature sensors (e.g. Meinen and Watts, 2000; Watts et al., 2001a; Meinen et al., 2004). In this new application of GEM fields to OI mapped IES data, the sources of error that will potentially influence the final accuracy of the gridded temperature, salinity, and density in comparison with point estimates of these quantities are as follows: the accuracy of the original measured IES travel time, the accuracy of the calibration of the travel time into $Z_{12}{}^*$, the errors in the OI mapping, and the scatter about the GEM fields. Previous work has shown that the first and second sources of error are small compared to the scatter about the GEM fields (e.g. Meinen and Watts, 2000). Throughout the rest of this paper the OI mapped values that are used are generally only those at grid points immediately adjacent to actual IES/PIES sites; the original OI mapping study showed that the errors in the OI mapped fields at the IES/PIES sites are extremely small (<2 m in Z_{12}) for all sites (Tracey et al., 1997; Watts et al., 2001b). As such, the accuracy of the temperature, salinity, and density estimated via the OI maps and the GEM fields is essentially dictated by the scatter about the GEM fields. As noted previously, the signal-to-noise ratios for salinity and density (not shown) are essentially the same as those for the temperature shown in Fig. 3.

The accuracy of the velocities estimated via these methods is somewhat more complicated to determine than for the property fields. Since the velocities (both relative and absolute) are determined geostrophically, they represent horizontal averages between the IES/PIES sites. As a result, the velocities at the IES/PIES sites within the array will have accuracies incorporating both the scatter about the GEM fields and the OI mapping accuracies for both $Z_{12}{}^*$ and pressure. While OI mapping procedures provide estimates of percent error variance (useful for array-design) based on input estimates of error variance at each site and of correlation length scales, it is difficult to determine the actual map accuracies in explicit dimensional units. The accuracy of the absolute velocities determined herein from the combined baroclinic and near-bottom reference level velocities was instead evaluated by comparison to direct velocity measurements from current meters (see Fig. 1a). As an example of the accuracy of the absolute velocities derived herein, Fig. 4 shows the directly measured zonal and meridional velocities at a central current meter mooring compared

Author's personal copy

with the PIES-GEM estimated velocities at the coincident location and pressure. Note that the current meter velocities shown are the measurements prior to correction for mooring motion (e.g., Cronin and Watts, 1996), and the PIES-GEM velocities that are compared were extracted from the four-dimensional grids of absolute velocity at the pressure measured by the sensors adjacent to the current meters on the mooring. This comparison could be done using the mooring motion-corrected current meter velocities, however this would result in a commingling of the accuracy of the PIES-GEM velocities and the errors in the mooring motion correction of the current meter velocities. Hence to eliminate that additional uncertainty, the absolute velocities derived herein are compared to the actual measurements made by the current meters at the pressure levels at which they were made.

The agreement between the PIES-GEM absolute velocities and the current meters is excellent, with correlation coefficients between 0.89 and 0.96 at the different levels/sites. The root-mean-squared (rms) differences are about 15 cm/s for the nominal 400-dbar sensors and 6 cm/s for the nominal 1000-dbar sensors. These rms differences represent only 7–9% of the peak-to-peak signals at these levels. More importantly for the mean fields presented in this paper, the differences between the PIES-GEM estimated mean currents and the current meter mean currents are generally only 2–3 cm/s at both depth levels. Because the PIES-GEM velocities represent a horizontal (geostrophic) average over the roughly 40–60 km distances between neighboring PIES while the current meters are true point measurements, the agreement is impressive. Support for the hypothesis that much of the

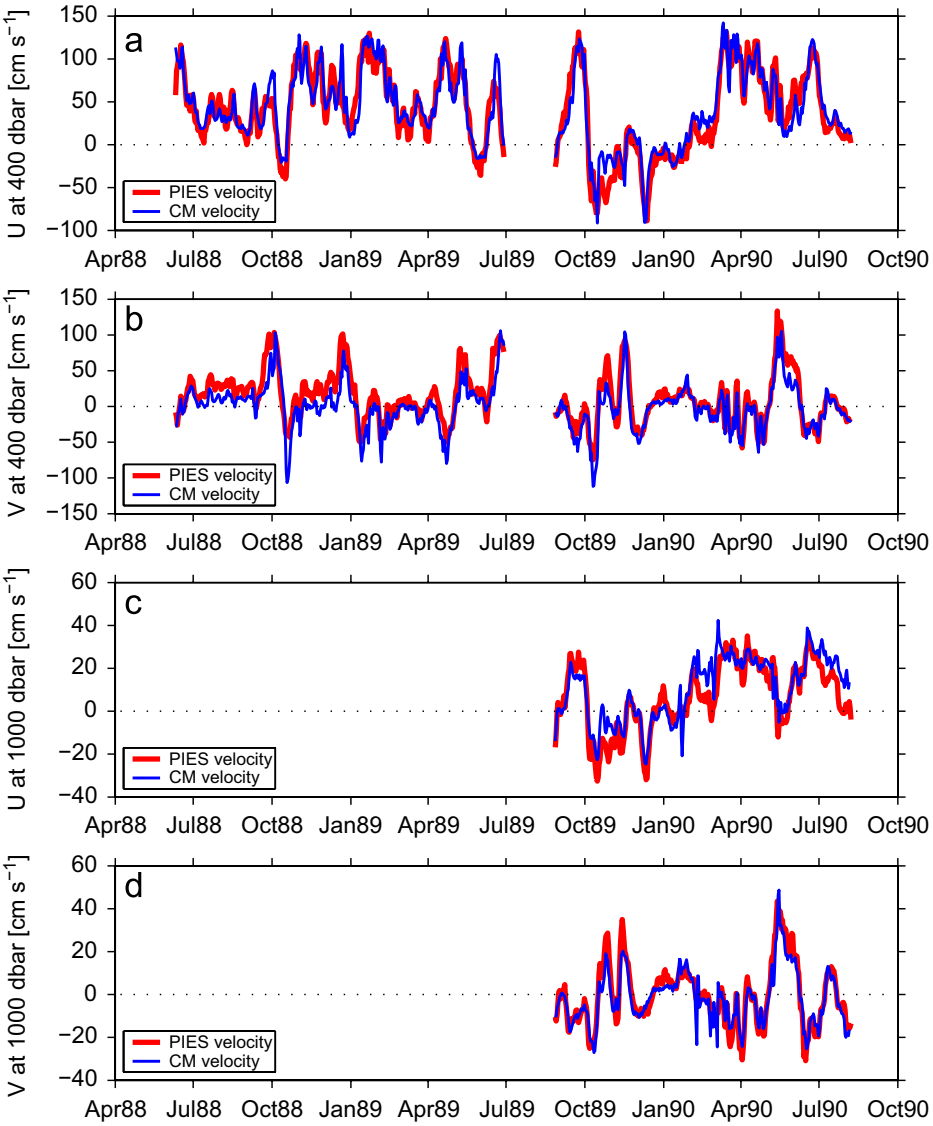

Fig. 4. Comparison of the directly measured velocities from the current meters at a central site in the SYNOP array (during two separate 1-year deployments) and the concurrent velocities estimated from the combination of the OI mapped IES travel times and the OI mapped bottom pressures. The current meter data have not been corrected for mooring motion, and hence contain variability reflecting downward deflections of the mooring that exceed 100 dbar at times. The PIES velocities are extracted from the full-water-column velocity profiles at the pressure levels measured by the sensors coincident with the current meters on the moorings. (a) Zonal velocity for nominal 400 dbar instrument; (b) meridional velocity for nominal 400 dbar instrument; (c) zonal velocity for nominal 1000 dbar instrument; (d) meridional velocity for nominal 1000 dbar instrument.

Author's personal copy

difference between the two velocity measurements is due to the horizontal averaging comes from a comparison of the high-frequency variance in the two quantities. The variance of the current meter records passed through a 10-day high-pass filter (second order Butterworth, passed both forward and backward to avoid phase shifting) exceeds that of the PIES-GEM velocities (filtered similarly) by 50–180%. This suggests there is much more high-frequency (presumably primarily small spatial scale) variability in the current meter data (note both current meter and PIES data has been 40-h low-pass filtered prior to the high-pass filtering). Similar agreement to that shown in Fig. 4 is found for comparisons of the PIES-GEM estimated temperatures and the moored temperature sensor values (not shown). Typical mean temperature differences for instruments at a nominal depth of 400 m (1000 m) are 0.2–0.4 °C (0.1–0.2 °C) and typical RMS temperature differences are 0.7–1.0 °C (0.3–0.4 °C); these differences are consistent with or smaller than the scatter about the GEM temperature field (see Fig. 3). The moorings did not have salinity sensors for comparison to the PIES-GEM estimates.

3.1. Stream-coordinates averaging

Averaging data in time as a function of position relative to a unique characteristic of a current, rather than as a function of geographic position, known as averaging in 'stream coordinates', is a well-established technique for determining the mean structure of a meandering current. While there are several different methods for averaging data from moored observation platforms in stream coordinates, each method has three steps in common: (1) define a unique characteristic of the current that will be used as the origin, the geographic position of which changes with time; (2) determine the cross-stream distance from the observation site to the nearest position of the origin at each time step; and (3) determine the direction of downstream flow so that the Cartesian velocity components can be rotated into along-stream and cross-stream components (e.g. Meinen and Luther, 2003). The specific methods applied to each of these steps vary from study to study, and the choices that are made affect the final results. Furthermore, as discussed in Appendix A, without a bit of subjective editing the final results can still have significant 'errors'.

Before describing how stream coordinates were applied to the SYNOP data in this study, a few comments regarding the data to be used are in order. As noted earlier, the combination of the OI mapping with the GEM has resulted in a four-dimensional grid of data at 20 km horizontal resolution. In theory each of the OI grid points could be used in the stream-coordinates averaging, however the OI grid points are not all independent from one another as noted earlier. More realistically the number of independent grid points within the array is defined by the number of independent time series going into the OI mapping. Therefore, the 13 grid points that most closely coincide with the 13 current meter moorings (and hence the PIES) were selected as the time series of profiles that would be used in the stream-coordinates averaging. This represents fewer than 10% of the total number of OI grid points available from the mapping (Fig. 1).

Stream coordinates averaging has been applied to the Gulf Stream in several studies at various places along the length of the current. In some of the earlier studies the origin of the stream-coordinate system was defined as the 'north wall', where the 15 °C isotherm crosses a depth of 200 m. Subsequent studies (e.g. Halkin and Rossby, 1985) showed that this choice was not optimal as having the origin out towards the flank of the current resulted in a noisier system. Having an origin other than at the center of the baroclinic core also will result in unwanted smoothing of the structure since the width of the current changes and the true structure 'pivots' about a central point. As such the hydrographic data from the region was used following the methods described in Meinen and Luther (2003) to define the Gulf Stream core, i.e., the origin, as the point where the 12 °C isotherm crosses 500 dbar. This is the same definition of the core used by JSBW95 in their stream coordinates averaging of the mooring motion-corrected current meter data. Cross-stream distance is defined as the distance from each observation site to the nearest point on the "Z_{12} equals 500 dbar" contour on each day. Once again this is the same definition used by JSBW95 and it is an 'improvement' over techniques which assume a 'frozen' cross-stream structure in order to determine cross-stream location. The 'frozen' field assumption was generally invoked by other researchers because of a lack of explicit information about where the origin was located each day (see Meinen and Luther, 2003, for a discussion of this point). For each of the 13 grid point time series, the cross-stream location is determined for each day. The observations of temperature and salinity are then averaged in 10 km wide bins starting from the bin centered on the core and moving out towards the cold 'north' side of the front and the warm 'south' side of the front (one additional step is required for the velocities before they too can be averaged into 10 km wide bins, as will be discussed shortly). No additional horizontal smoothing (beyond the 10 km bin averaging) is applied to the sections (except for the cross-stream velocity as will be discussed shortly). Only bins that contain at least 25 observations are kept, which restricts the useful domain to bins centered between 140 km towards the cold side of the front and 150 km towards the warm side of the front.

The definition of downstream direction needed to rotate the velocity observations into the along- and cross-stream components is more problematic. As discussed in both JSBW95 and Meinen and Luther (2003), there are basically two ways to define the direction of downstream flow for each moored observation site. First of all, the tangent to the 'Z_{12} equals 500 dbar' contour at the point of closest approach can be used (see Fig. A1). Second, the velocity shear between the upper levels can be used to determine the downstream direction by defining it as the direction in which there is the maximum vertical shear in horizontal velocity. The JSBW95 study discussed some of the advantages and disadvantages of these two

Author's personal copy

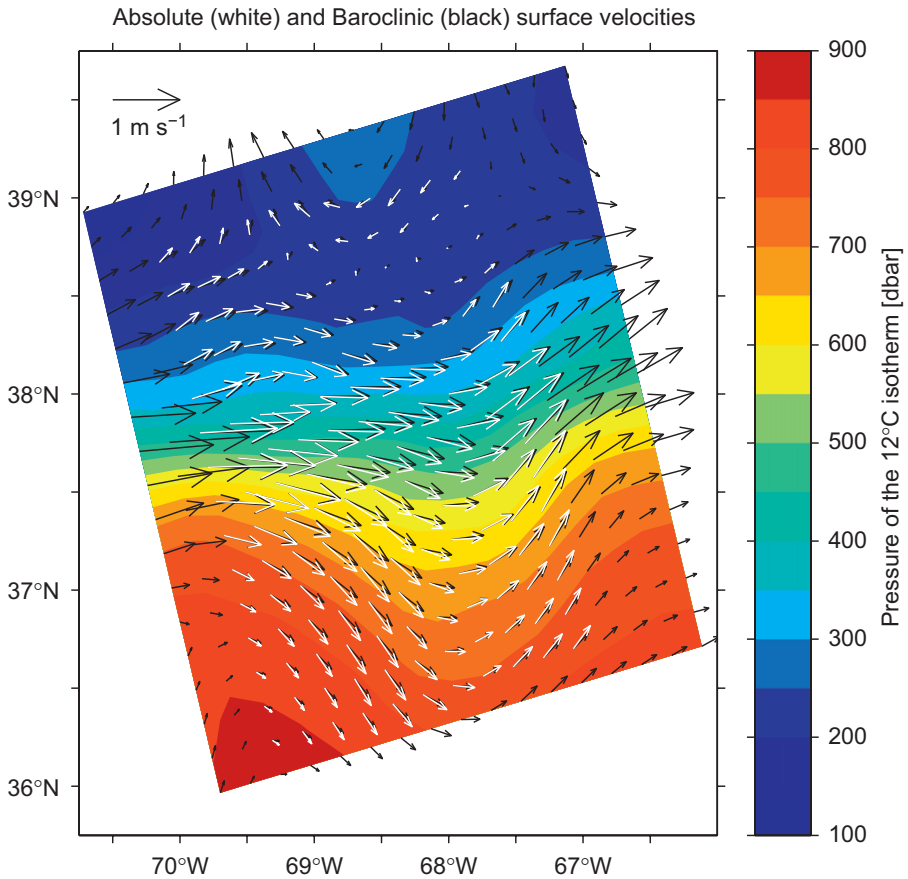

Fig. 5. Record-length-mean surface geostrophic velocity (vectors) and thermocline depth (color contours). Thermocline depth is illustrated using the pressure of the 12 °C isotherm. Both absolute velocity (white vectors) and velocity relative to 3500 dbar (black vectors) are shown. Absolute velocities are available over a smaller domain due to the smaller coverage of bottom pressure sensors (see Fig. 1).

techniques, and they chose to use a hybrid of the two methods, utilizing the vertical shear technique whenever the shear between the 400 and 1000 dbar instruments was greater than 5 cm/s and the tangent method when the shear was less than 5 cm/s. A primary concern with the vertical shear method is that this forces all of the baroclinic velocity structure into the downstream direction *a priori*, while it would be preferable to determine this as a result rather than as an assumption. As will be shown shortly, the assumption is misleading for the Gulf Stream at this location and leads to large differences in the velocity structure, particularly at the flanks of the Gulf Stream.

4. Results

Consistent with the original studies of the SYNOP data (e.g. Lindstrom and Watts, 1994; Watts et al., 1995; Lindstrom et al., 1997), the present study finds that the 2-year mean of the circulation within the Central Array shows a weak meander-trough structure with the absolute velocity vectors turned slightly clockwise of the relative velocities (relative to a level of no motion at 3500 dbar) entering the trough, consistent with downwelling, and absolute velocity vectors turned slightly counter-clockwise of the relative velocities exiting the trough, consistent with upwelling (Fig. 5). The maps of thermocline depth/pressure are essentially identical to those produced by Watts et al. (1995). However, where that study obtained velocity only from four levels of mooring motion-corrected current meter data at 13 sites (see also Cronin and Watts, 1996), the present study has absolute velocities at a much more complete 10 dbar vertical resolution and 20 km horizontal resolution.[4] Furthermore the velocities herein, as geostrophic estimates, are by their very nature dynamically consistent with the temperature and salinity fields, unlike the point current meter measurements, especially where the current meter data were interpolated or extrapolated to other depth levels than the nominal four. The geostrophic derivation can, of course, also be a drawback as any ageostrophic velocities are missed by the PIES-GEM technique, but the overall agreement with the non-mooring-motion-corrected current meter velocities suggests that this is not a major liability. The Eulerian mean sections extracted along the central line of the array

[4] Note that given a 50–60 km correlation length scale (e.g., Tracey et al., 1997) not all of the horizontal grid points are independent. Regarding the independence of the vertical grid points, the hydrographic data that was used to create the GEM field had 1–2 dbar vertical resolution, so the measurements themselves are independent of one another although given the varying vertical correlation length scale in the ocean the levels themselves are not independent of one another.

Author's personal copy

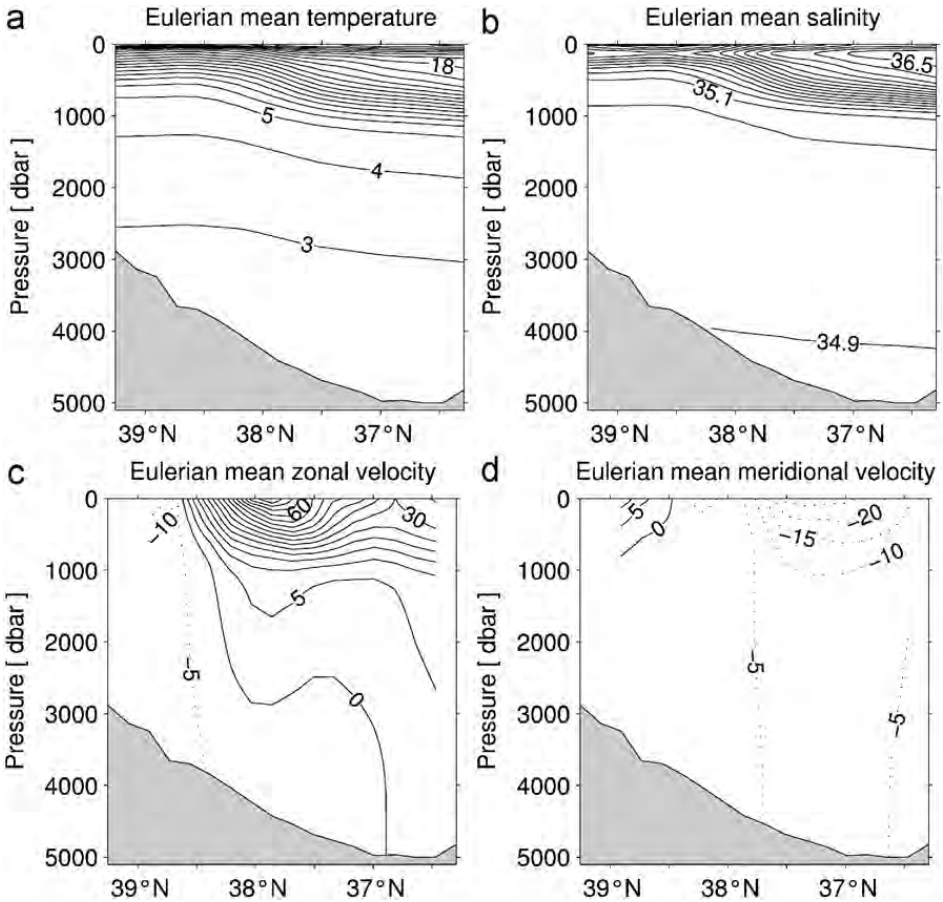

Fig. 6. Eulerian mean sections calculated at the grid points along the central line of the array using the full lengths of the records. (a) Temperature (°C); (b) salinity; (c) zonal velocity (cm s^{-1}); (d) meridional velocity (cm s^{-1}).

(Fig. 6) show a broad, smooth front and a multiple-core velocity structure, which is not unexpected when Eulerian averaging is used in the presence of a strongly meandering current like the Gulf Stream (JSBW95). To get a better picture of the mean structure of the Gulf Stream during this 2-year period a different averaging approach is needed, that of 'stream coordinates' averaging.

4.1. Stream-coordinate mean temperature, salinity and velocity sections

The stream coordinates mean section of temperature (Fig. 7) shows the thermocline dipping from around 150 dbar on the cold 'north' side of the front to about 850 dbar on the warm 'south' side of the front. The thick layer of 18 °C mode water expected in this region (e.g. Worthington, 1959) shows up strongly with fairly constant temperatures found from 200 dbar down to near 500 dbar, increasing in depth and thickness to the south of the Gulf Stream core. The uniform nature of this layer is much more pronounced in the stream coordinates section (Fig. 7) than in the Eulerian mean section (Fig. 6a). The warm core of water greater than 25 °C is found right at the stream coordinates origin above 100 dbar. The largest standard deviations of the stream coordinates temperatures are found just north of the core near the surface (Fig. 7), while at depth the highest standard deviations are associated with the strongest gradients in temperature, as expected.

To determine the standard error of the mean, and hence the statistical accuracy of this mean section, the standard deviation should be divided by the square root of the number of degrees of freedom in the record. Analysis of the 12 bottom pressure records and 24 travel time records from the PIES and IES finds that the average Eulerian integral time scale (e.g. Emery and Thomson, 1998) of all of the instruments is about 23 days (see Appendix B). Previous studies of the Gulf Stream have shown that the integral time scale in stream coordinates is essentially the same as the integral time scale in Eulerian coordinates (e.g. JSBW95). Utilizing the definitions of degrees of freedom and integral time scales applied herein, two integral time scales are required to provide a single degree of freedom (see Appendix B for details). However this does not imply that each of the 10 km wide stream-coordinates bins has a number of degrees of freedom equal to the length of the record divided by twice the integral time scale, because the data within each 10 km bin are sporadic in time depending on the distance on any given day from an observation site to the core of the Gulf Stream, with the outermost bins having as few as 25 daily observations during the entire 2-year record. Insofar as the limited observations within each bin are

Author's personal copy

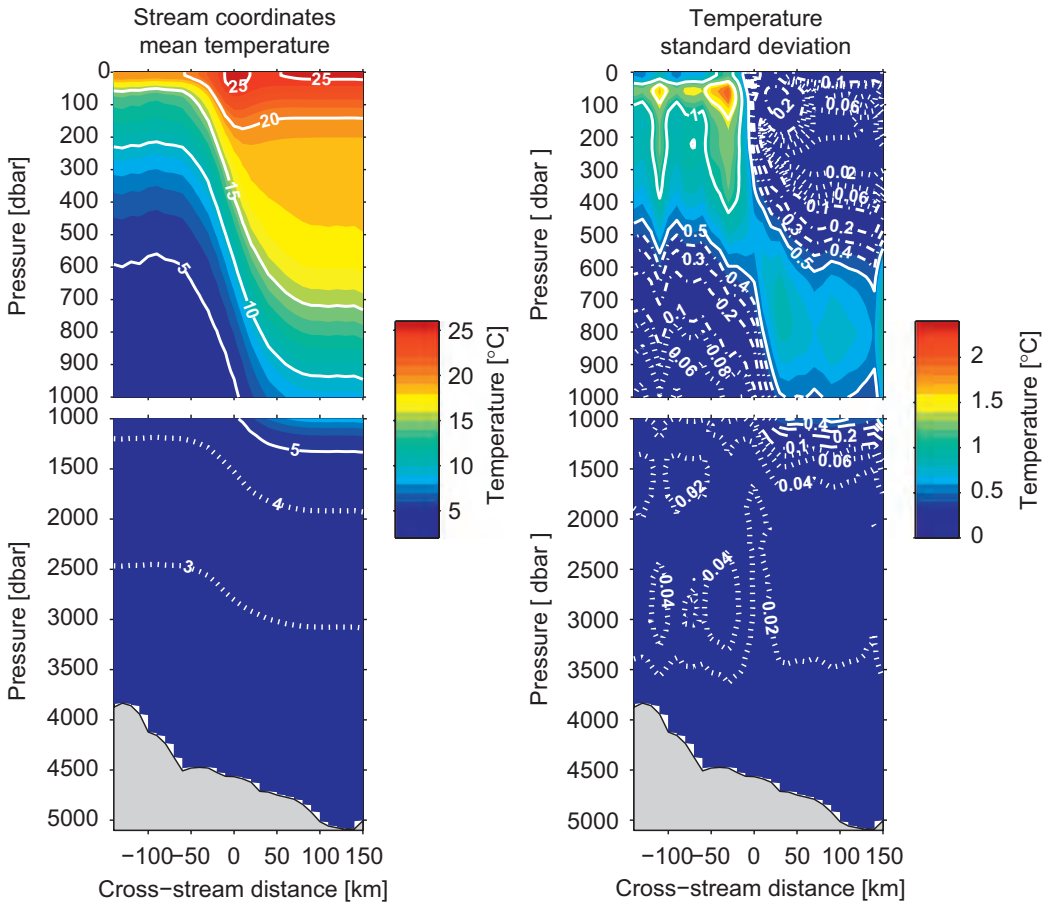

Fig. 7. Left panels: stream coordinates mean temperature section; see text for details of calculation. Note the two different contour intervals. Gray filled bottom is based on a weighted average of the actual depths of the OI grid points, with the weighting based on the number of observations from each OI point that contributed to the stream coordinates average in each 10 km wide bin. The total number of points averaged in each 10 km bin ranges from just over 30 on the flanks to just under 600 at the core. Right panels: standard deviation of the stream coordinates values. Note the three different contour intervals.

separated in time by less than the temporal decorrelation scale, they would not be independent of one another. To estimate the number of degrees of freedom available in each 10 km wide bin, the complete record was broken up into 46 day segments (two integral time scales) and the number of 46 day segments which included at least one observation was summed for each 10 km wide bin. Computed this way, the number of degrees of freedom ranges from only 4 in the bin centered at +150 km along the warm side of the front to values between 15 and 17 in the bins near the core (between −90 to +90 km) down to about 9 in the bin centered at −140 km along the cold side of the front. Therefore, the standard error of the mean can be found by dividing the standard deviations shown in Fig. 7 (right panels) by 2–3 (the square root of the number of degrees of freedom) at the flanks and by about 4 near the core of the current.

The stream-coordinates mean section of salinity (Fig. 8) shows the Gulf Stream as a boundary between the saline ($S>36$) waters to the south ('warm' side) of the Gulf Stream and the cold and fresh waters to the north. The salinity maximum on the cold side of the front is found centered near 125 dbar with value of 35.45, with fresher waters both above and below. The peak salinity value of 36.70 is found at 120 dbar just a few kilometers towards the warm side of the front, again suggesting that the core definition used herein is robust. The highest standard deviations of salinity are found at the surface[5] on the cold side of the front, with peak values following the halocline downwards towards the warm side of the front (Fig. 8). The standard error of the mean is the standard deviation in Fig. 8 divided by approximately 2–3 along the flanks and 4 between ±90 km (as with the temperature section). Note that the earlier JSBW95 study made no effort at estimating a stream-coordinates mean salinity section as the moorings did not have the required high quality conductivity sensors.

The stream-coordinates mean section of along-stream velocity (Fig. 9) shows the classical offshore shift of peak velocity with increasing depth found in nearly all previous stream-coordinates sections of the Gulf Stream in this region, such as that by Halkin and Rossby (1985) at 73°W and JSBW95 at 68°W (but it was not found by Bower and Hogg (1996), at 55°W, perhaps because that section had

[5] Note that the fact that the highest salinity standard deviations are found right at the surface while the temperature standard deviations have a maximum at 50 m suggests that precipitation effects may be increasing the observed salinity variance in the stream coordinates salinity data.

Author's personal copy

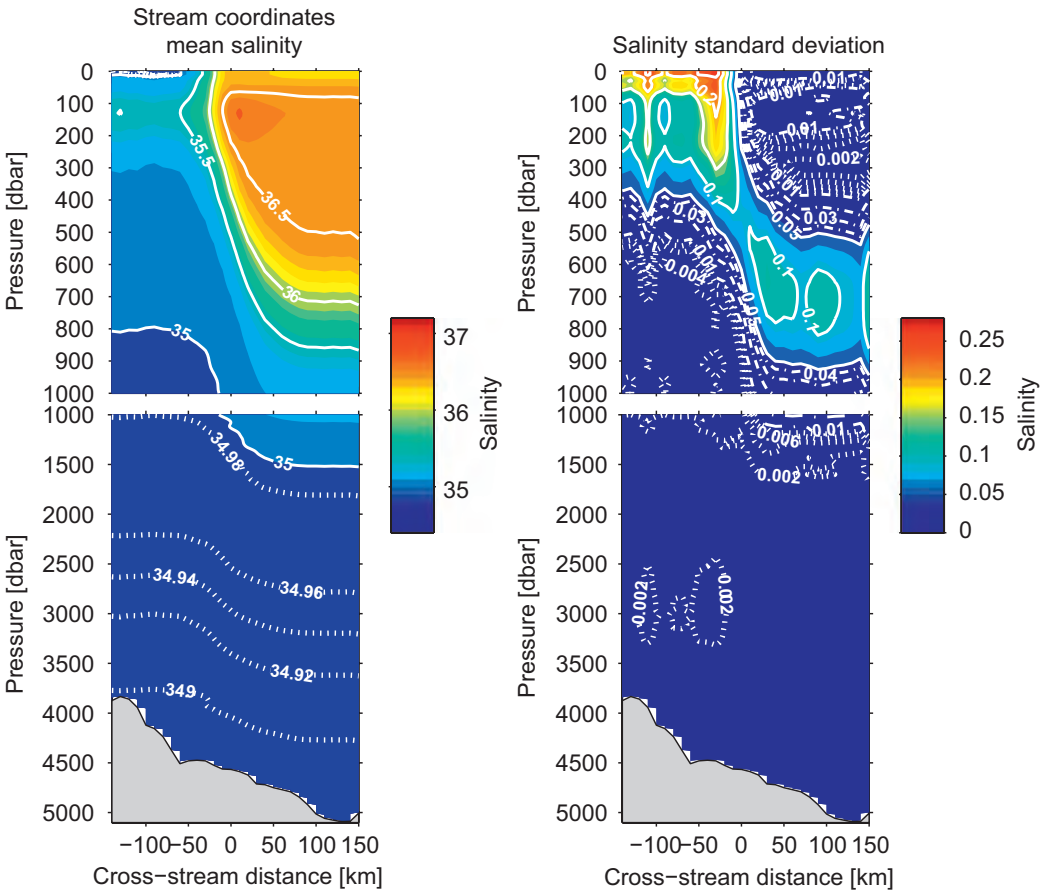

Fig. 8. Left panels: stream coordinates mean section of salinity. Note the two different contour intervals. The bottom is as described in Fig. 7. Right panels: standard deviation of the salinities. Note the three different contour intervals.

no data above 500 m). Peak velocities of just over 170 cm/s are found at the surface about 15 km north ('cold' side) of the stream-coordinates origin, while peak velocities at 400 dbar are found at about 15 km on the warm 'south' side of the origin. The peak standard deviations of the along-stream velocity follow a similar pattern, trending deeper with increasing offshore distance (Fig. 9). The zero velocity contours (thick white lines in Fig. 9) bound a current that is about 155 km wide at the bottom and more than 230 km wide at the surface (there is a small amount of near-surface downstream flow that is missed on the warm side of the current due to an insufficient quantity of data). The current is somewhat wider near the surface than was observed by JSBW95 using the current meter data, and there are slightly stronger eastward currents below 1500 m (i.e., stronger barotropic flow) than observed by JSBW95. These velocity differences are statistically significant, at the 95% level based on the estimated error bars and the number of degrees of freedom, and they illustrate the importance of the hydrography-based shear between 1000 and 3500 m inherent in the GEM technique versus the simple interpolation possible between these two depths in the current meter data used in the JSBW95 study. It is shown in the Appendix A that the greater than 5 cm/s counter-flow found 150 km south ('warm' side) of the core by JSBW95 appears to be an artifact of including observations within cold core rings in the stream-coordinates calculations for the Gulf Stream. In fact the result of stream-coordinates averaging the PIES data with the ring data included is visually identical to the JSBW95 section. Direct comparison with the JSBW95 section is not possible because the numerical values used to make their mean section plot have been lost (W. Johns, personal communication, 2005).

The mean along-stream transport of the Gulf Stream in stream coordinates is 117 Sv (integrated between zero velocity contours). Following the methods described in Meinen and Watts (2000), the accuracy of the mean transport is a function of both any possible errors in the measurement system and the statistical accuracy of the calculation of the mean (i.e., the standard error of the mean). The measurement accuracy (one standard error level) of a daily section of transport is about 13 Sv (taking into account the hydrographic scatter about the GEM fields and the direct measurements of travel time and pressure), and given the dominant 23-day time-scale observed herein (see Appendix B) the total accuracy (measurement plus statistical accuracy, one standard error level) of the mean transport is estimated to be about 3 Sv. Therefore, the transport value of 117 Sv is not statistically different at 95% confidence from the 113 Sv value determined by JSBW95 from the SYNOP current meter data. If real the larger transport represents a 20% larger inflow rate (4.4 Sv per 100 km) from 73°W than has

Author's personal copy

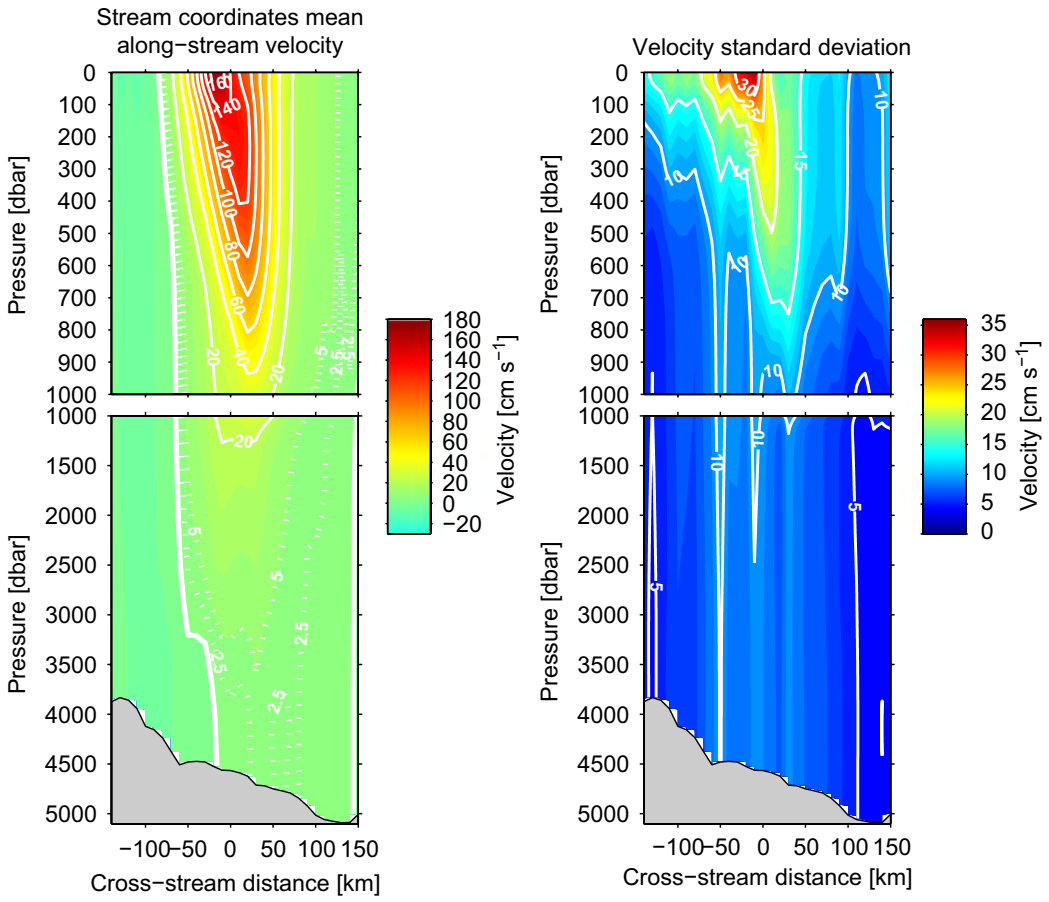

Fig. 9. Left panels: stream coordinates mean section of along-stream velocity. Note the two different contour intervals. Thick white contours denote zero velocity. The bottom is as described in Fig. 7. Right panels: standard deviation of the along-stream velocity.

previously been estimated (JSBW95). A comparison of the along-stream transport as a function of depth from the present study and the JSBW95 study (where the latter was hand-digitized from the figure in their paper) illustrates that the excess transport results from slightly stronger transports above 600 m and slightly stronger transports between 1800 m and the bottom (Fig. 10). Much of the difference in actual structure occurs below 1000 m, where JSBW95 were essentially interpolating between the 1000 and 3500 m current meters. Inside this layer JSBW95 generally had no data unless mooring motion pulled down the nominal 1000 m instruments into the upper few hundred meters of this layer. The PIES-GEM velocities, on the contrary, utilize real hydrographic data to evaluate the structure between these two depths.

The stream-coordinates mean of the cross-stream velocity demonstrates that 68°W is a region of inflow into the Gulf Stream (Fig. 11), consistent with previous studies of the circulation in this area (e.g. Hogg, 1992; JSBW95). The strongest inflow is found to occur on the south ('warm' side) of the Stream and below 1000 m, perhaps explaining the greater width and increased barotropic flow found farther downstream at 55°W (Bower and Hogg, 1996), although it may also simply reflect a more local process. The cross-stream velocities are somewhat noisier than the along-stream velocities, so for this quantity a 30 km centered running mean filter has been applied to smooth the stream-coordinate mean section horizontally (the filter was applied after stream-coordinate averaging). The zero-contour (thick white line in Fig. 11) is not centered on the core of the downstream flow, but rather is shifted about 50–60 km towards the south flank of the current. The peak mean velocities are quite low, only 2–5 cm/s near the surface and rarely exceeding 3 cm/s at depth. Note the weak, but non-zero, vertical shear in these velocities. Had the vertical shear definition of the downstream flow direction been used in the stream-coordinate calculation, as was done in most cases by JSBW95, these baroclinic shears would have been rotated into the along-stream direction. The largest variability (Fig. 11, right panels) is confined above 1000 dbar except for a band centered 50 km towards the cold side of the front. This latter feature may be a sign that some warm-core ring data erroneously slipped into the stream-coordinate averaging despite the hand editing discussed in Appendix A. This possible artifact does not affect the observation of confluent flow on the south side of the current. The vertical mean cross-stream velocities (not shown) have peak inflows of 2–3 cm/s at roughly 100 km on either side of the front. These values are only marginally different from zero at a one standard error level and are not significantly different from zero at 95% confidence. Nevertheless, given a rough mean depth of 4500 m this inflow, if real, would translate to a convergence of about 18–27 Sv per 100 km (not inconsistent with JSBW95's estimate of ~18 Sv per 100 km inflow at this

Author's personal copy

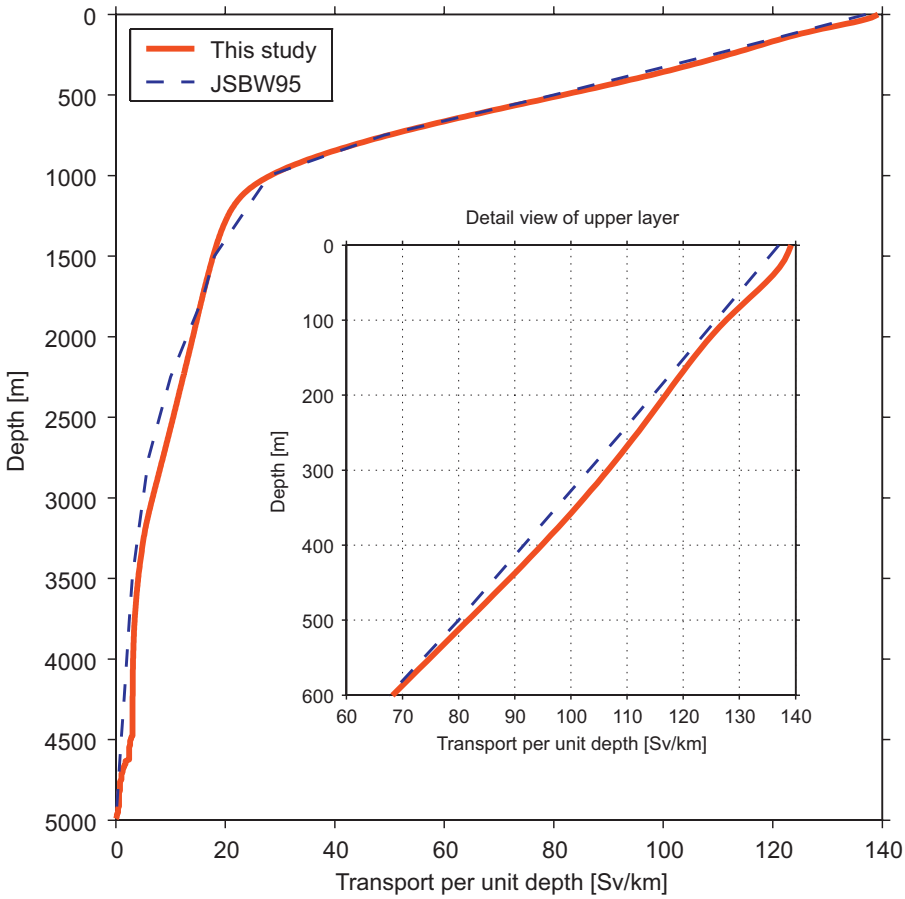

Fig. 10. Along-stream transport (integrated between the zero contours) as a function of depth. Both the values from the present study and the values from JSBW95 are shown (see legend for line-types). Values for JSBW95 were hand digitized from the figure in their paper. Inset panel shows the details of the upper 600 m.

longitude from the SYNOP moored current meter data). This value is about 5–7 times larger than the bulk inflow value of 4 Sv per 100 km that would be determined using the estimates of along-stream transport upstream at 73°W (Leaman et al., 1989) and downstream at 55°W (Hogg, 1992), possibly indicating that this is a local 'hot-spot' for inflow into the Gulf Stream.

4.2. Potential vorticity structure of the Gulf Stream

In the absence of direct forcing and dissipation, water parcels will always strive to conserve their potential vorticity (e.g., Gill, 1982), which can be represented in a stratified fluid as

$$\frac{D}{Dt}\left(\frac{1}{\rho}\frac{\partial\sigma_\theta}{\partial z}(f+\zeta)\right)=0$$

where ρ, σ_θ, f, and ζ are the density, potential density, Coriolis parameter, and the vertical component of the relative vorticity, respectively. Due generally to insufficient data, most studies of the potential vorticity neglect the relative vorticity entirely or approximate it as only the cross-stream gradient of the along-stream velocity. Some studies have attempted to determine the complete relative vorticity component, but these are generally snapshots from hydrographic/ship-based surveys (e.g., Hummon and Rossby, 1998). Rossby and Zhang (2001) estimated the potential vorticity of the Gulf Stream at about 71°W in stream coordinates using high horizontal resolution data from repeat sections with an Acoustic Doppler Current Profiler installed in a freighter. The Rossby and Zhang (2001) results, however, were limited to the upper 200–250 m and they were unable to evaluate the along-stream gradients. The data set presented herein provides the opportunity to do something that has not been done in the past to the authors' knowledge, that is, calculate the time-varying complete relative vorticity in stream coordinates including the downstream evolution of the cross-stream velocity, and provide a complete vertical section of the total stream-coordinates mean potential vorticity.

The along-stream gradients of velocity were determined as follows. For each observation site on each day the cross-stream location and direction of downstream were determined as discussed previously for the stream-coordinates averaging. For each site on each day the corresponding three-dimensional grids of velocity were used to interpolate and find the velocity that was observed precisely 10 km in the downstream direction from the original observation site. This procedure was then used to find the observed velocity precisely 10 km upstream of the original observation site. The upstream velocity estimates were then averaged based on the cross-stream location of the original observation site and

Author's personal copy

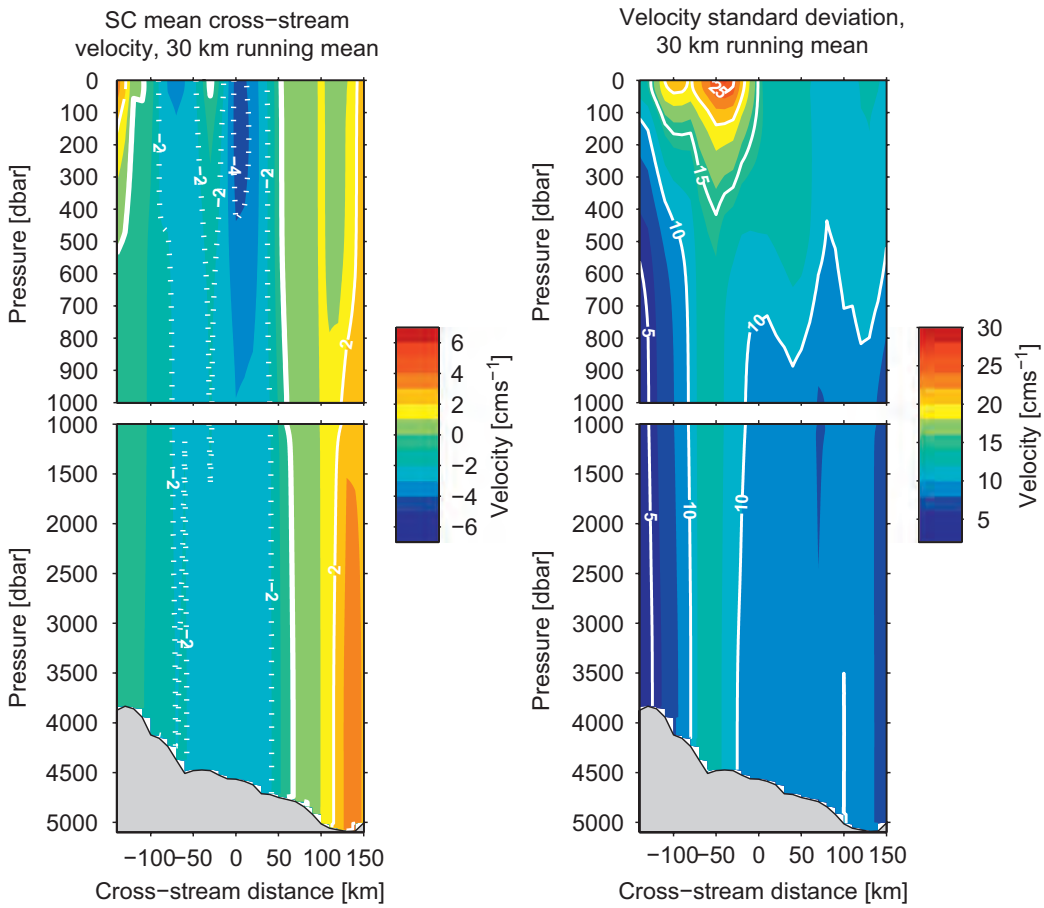

Fig. 11. Left panels: Stream coordinates mean section of cross-stream velocity. Because the cross-stream velocity is noisier than the along-stream, the mean field has been smoothed with a 30 km centered running mean. Thick white contour denotes zero velocity. The bottom is as described in Fig. 7. Right panels: Standard deviation of the cross-stream velocity, also smoothed with a 30 km running mean.

so were the downstream velocities, essentially creating a stream-coordinates mean upstream section and a stream-coordinates mean downstream section. The differences between these two sections, divided by the 20 km distance between them, provides a centered difference estimate of the along-stream gradient of velocity. The cross-stream gradient of the along-stream velocity was calculated as the cross-stream gradient of the data in Fig. 9. The relative contributions of the two terms to the total relative vorticity can be illustrated by studying their ratios as a percentage of the planetary vorticity (Fig. 12). The cross-stream gradient of along-stream velocity (Fig. 12, top) is the larger of the two components, with values reaching up to 30% of the planetary vorticity in the upper few hundred dbar. This term has stronger magnitudes on the cold side of the core than the warm side by a factor of about 1.4. The along-stream gradient of cross-stream velocity (Fig. 12, middle), while much smaller, is not negligible with a maximum value of just over 12% of f about 30 km towards the cold side of the core. The along-stream gradient of cross-stream velocity has no significant values on the warm side of the core. While the two components are somewhat asymmetric about the core the total relative vorticity, calculated as the difference of the two terms, has a more symmetrical peak magnitude of 28–32% of the planetary vorticity on either side of the core, although the strongest values are shallower on the cold side of the core (Fig. 12, bottom).

The potential vorticity (PV) calculated with the full relative vorticity demonstrates higher values on the cold side of the core, particularly in the upper 100 dbar (Fig. 13). The PV front that shifts offshore with depth due to the offshore shift of the pycnocline (light gray contours) is enhanced by the relative vorticity associated with the velocity maximum that also shifts offshore with increasing depth (Fig. 9). Below 1000 dbar the PV values drop several orders of magnitude below the values above 100 dbar. The higher horizontal velocity shear on the cold side of the front in the upper water column, and hence the higher ζ and PV, is consistent with the shipboard ADCP results presented by Rossby and Zhang (2001) just west of the SYNOP study region at 71°W. The PV structure in the SYNOP region is also fairly similar to that derived from a 3-layer analytical model of the PV that used hydrographic and Pegasus data in the Gulf Stream at about 73°W (Logoutov et al., 2001) although the amplitudes of the relative vorticity appear to be a bit lower at 68°W. This lower amplitude may be due to the use of geostrophically-averaged velocities (over the span between OI grid points) as opposed to direct velocity measurements as were used in the Logoutov et al. (2001) study, although the close agreement of the PIES-GEM absolute velocities (Fig. 4)

Author's personal copy

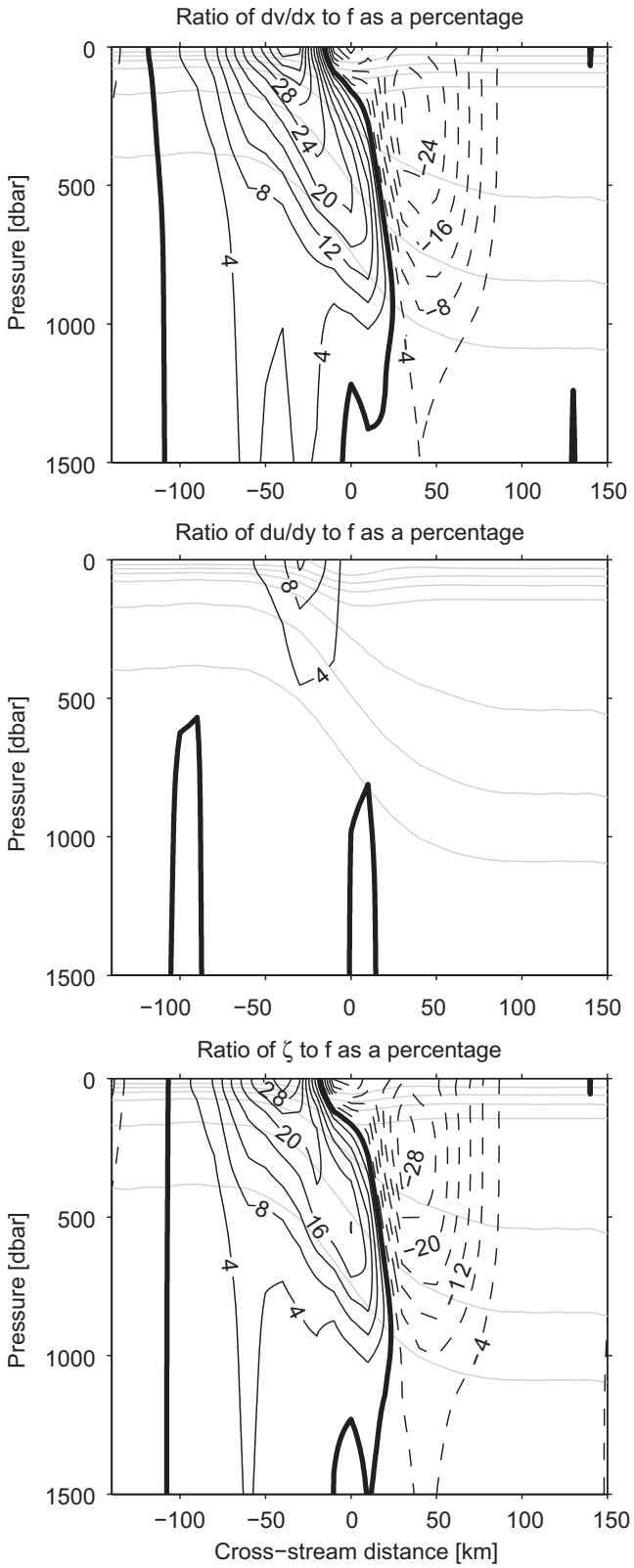

Fig. 12. Comparison of the relative and planetary vorticity. Top—the cross-stream gradient of along-stream velocity as a percentage of *f*. Middle—the along-stream gradient of cross-stream velocity as a percentage of *f*. Bottom—the complete relative vorticity ($dv/dx - du/dy$) as a percentage of *f*. Thick black contours indicate zero; dashed contours indicate negative values. Only the upper 1500 dbar are shown as deeper values are all quite small. Light gray contours indicate potential density (relative to surface) in 0.5 kg m^{-3} intervals, with the largest contour shown being 27.5 kg m^{-3}.

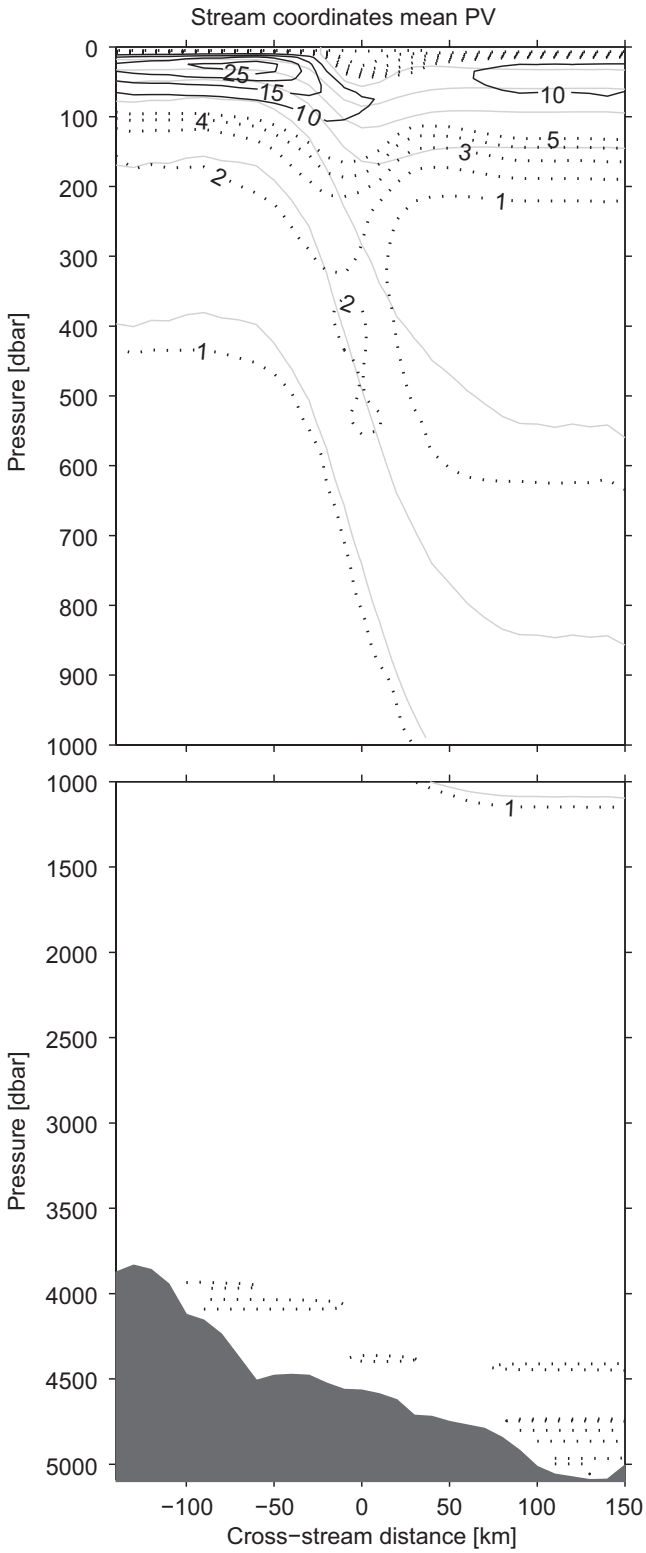

Fig. 13. Stream coordinates mean potential vorticity (including the complete relative vorticity). Units are 10^{-10} m^{-1} s^{-1}. Note that solid and dotted contours represent contour intervals of five and one respectively. Gray filled bottom is as described in Fig. 7. Light gray contours indicate potential density (relative to surface) in 0.5 kg m^{-3} intervals, with the largest contour shown being 27.5 kg m^{-3}.

with direct measurements suggests that this 'problem' cannot be particularly severe. Regardless, the inclusion of the complete relative vorticity and the temporal averaging

Author's personal copy

possible due to the time-series nature of the observations makes the PV structure derived herein one of the most accurate pictures of the mean PV of the Gulf Stream ever produced.

5. Conclusions

The results herein provide new detailed vertical sections of properties of the Gulf Stream centered about 68°W, and they illustrate that these kinds of observations can be made at a much lower cost than is required for a large array of tall current meter moorings (~$25 K for a PIES compared to ~$150 K or more for a mooring depending on the number and types of instruments placed on the mooring). The resulting temperature, salinity, and velocity sections are by definition dynamically consistent with one another, and they suggest that the mean Gulf Stream is slightly broader than had been thought, with a mean width of about 250 km at the surface and 155 km at the bottom. The mean transport for the SYNOP period was 117 Sv, just a few percent larger than the 113 Sv transport determined by JSBW95 using the mooring motion-corrected current meter data from SYNOP. The excess transport is evenly split between the baroclinic and barotropic components (where barotropic is defined as the bottom velocity multiplied by the water depth following Fofonoff (1962); under the alternate definition of barotropic as the vertical mean all of the transport is barotropic by definition). The recirculation gyres on either side of the Gulf Stream have a baroclinic component although it is fairly small, perhaps 10% of the total. The bulk rate of inflow between 73°W and 68°W appears to be about 20% stronger (at 4.4 Sv per 100 km) than had been believed in the past based on previous studies of the SYNOP data (JSBW95). The local inflow rate may be even larger, 20 Sv per 100 km, possibly indicating that 68°W may be the location of a maximum of the inflow. The PV structure has a non-negligible contribution from the along-stream gradient of cross-stream velocity. The structure of the mean PV field found herein is similar to that found in the upper 200 m at about 71°W from repeat shipboard ADCP sections (Rossby and Zhang, 2001).

Acknowledgments

Rigoberto Garcia provided a great deal of help with the stream-coordinates calculations done for this study, and he also made a number of useful suggestions for improving an earlier draft of this manuscript, as did Tom Rossby, Randy Watts, and two anonymous reviewers. Karen Tracey and Randy Watts at the University of Rhode Island and Bill Johns at the University of Miami were all very helpful in providing both information about the SYNOP program and the associated SYNOP data. Special thanks also to Karen Tracey and Randy Watts for providing the OI mapped fields. Helpful interactions with Randy Watts, Rick Lumpkin, and David Enfield, aided in the discussion of integral time scales and degrees of freedom. This research was supported by the National Science Foundation under grants 0352256 and 0352229 and by the NOAA Atlantic Oceanographic and Meteorological Laboratory.

Appendix A. Stream coordinates in a complex environment

As discussed in the main body of the text, the conversion of Eulerian data into stream coordinates proceeds by determining the distance to the nearest point of approach of the current core, herein defined as the 'Z_{12} equal to 500 dbar' contour. The challenge in this is that there may be more than one such contour within the array domain, such as occurred on December 8th, 1989 (Fig. A1). When there are multiple contours within the array, this is a sign that a complicated flow may cause difficulty in the calculation of stream-coordinates position and the direction of downstream flow that should be applied for the different observation sites. Consider the observation site indicated by the gray square in Fig. A1. The default determination for the cross-stream location might be that indicated by the gray dashed line, however it is clear that the flow at that observation site is far more likely to be dominated by the cold core ring that is right on top of the site than by the main Gulf Stream flow more than 100 km away. It is a somewhat subjective decision as to whether such observations as the example indicated in Fig. A1 should be used or not in building the stream-coordinates average. In one sense the existence of rings on either side of the current is something that does contribute to the mean circulation of the region and thus should not be neglected. On the other hand the goal of stream-coordinates averaging is to determine the 'best possible'

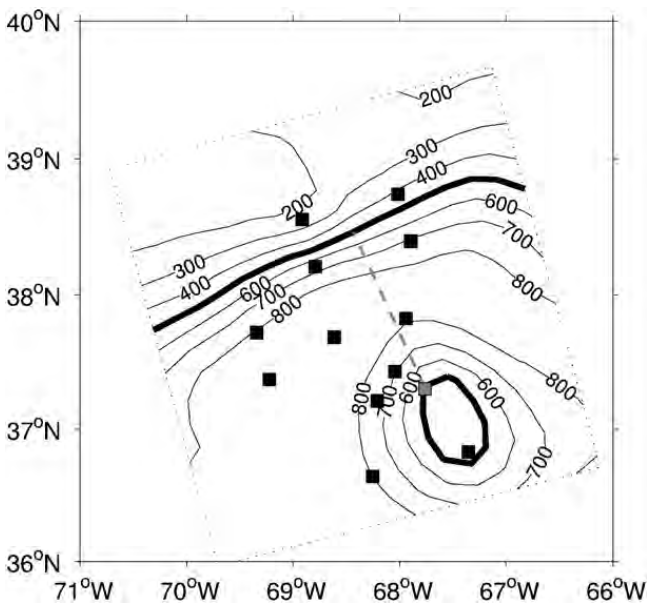

Fig. A1. Contoured field indicates the pressure of the 12 °C isotherm on December 8th, 1989. Bold lines denote the 500 dbar contours. Squares denote the locations of the OI grid points used for stream coordinates averaging (each square neighbors one of the current meter moorings). The gray dashed line illustrates the method for defining the stream coordinates cross-stream location for the mooring denoted by the gray square. Note that this square illustrates a mooring for which the measured values will be heavily influenced by the cold core ring present on this day.

Author's personal copy

picture of the structure of the current itself, not features that are semi-independent such as rings that have broken off of the main current, and thus observations such as that made at the site indicated by the gray square in Fig. A1 should not be used in making the stream-coordinates average. The decision made in this regard can have a significant effect on the final result, as is illustrated by the two mean along-stream velocity pictures shown in Fig. A2. In Fig. A2a all data have been used, while for Fig. A2b the data used in making the stream-coordinates mean section have been carefully selected by hand in order to exclude data from rings or filaments. The difference between the two sections is shown in Fig. A2c. Near the core of the Gulf Stream there is little difference in the two sections; the principle differences appear out at the flanks as expected. Excluding the ring and filament data has resulted in a wider along-stream flow at the surface and the elimination of a potentially spurious strong counter-flow on the warm flank of the current. There is a similar change on the cold side of the front, but it is much smaller possibly

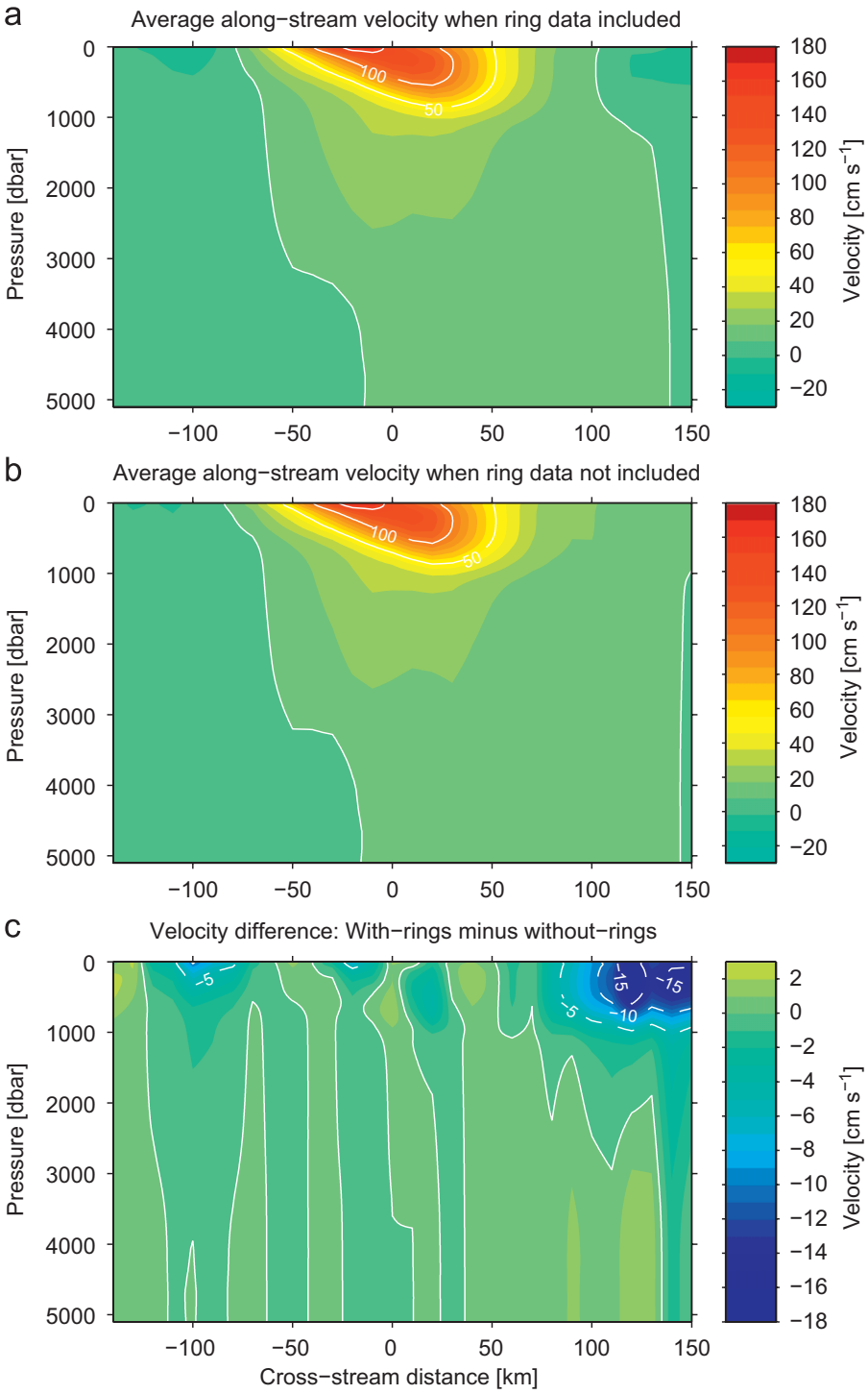

Fig. A2. Stream coordinates mean along-stream velocity: (a) the average when all observations are used; (b) the average when data from rings and other filaments are excluded; (c) the difference, with panel (b) minus panel (a). White contours denote zero velocity.

Author's personal copy

reflecting the fact that the mean current was passing further north in the array so that there are fewer observations on the cold side of the front in rings than on the warm side. The decision made in this study was to exclude data within rings and filaments when making the stream-coordinates averages. Note that the counter-flow on the warm side of the current is found in the mean velocity section of JSBW95, consistent with that study not having removed the ring and filament data during stream-coordinates averaging.

Appendix B. Calculating degrees of freedom and integral time scales

The calculation of degrees of freedom (DOF) and integral time scales (ITS) from time-series observations are standard tasks in the statistical analysis of the data, however, there are inconsistencies in the definitions of these quantities and their relationship with one another in the oceanographic literature. As such it is imperative that these quantities be defined within each paper so as to be clear about how DOF and ITS determined in one study should be compared to those determined in another. This appendix reviews briefly the different definitions and points out the inconsistencies between them.

The DOF is commonly defined (e.g., Davis, 1976) as proportional to the inverse of the integral of the autocorrelation over lags from minus infinity to positive infinity:

$$\mathrm{DOF} = T\left(\int_{-\infty}^{+\infty} R(\tau)\mathrm{d}\tau\right)^{-1} \tag{B.1}$$

where T is the length of the time record, R is the autocorrelation, and τ is the lag. The key to note here is that the integral is from lags of $-\infty$ to $+\infty$. There is little disagreement in the literature about this definition of DOF, and it can be found in numerous research papers and textbooks (e.g., Davis, 1976, 1977; Sciremammano, 1979; Bendat and Piersol, 1986; Emery and Thomson, 1998). The complication comes not from the definition of DOF but from the definition of the ITS and its relationship to DOF.

The definition of ITS used by Davis (1976) can be written as the following, where the notation has been converted from discrete to continuous and has been simplified a little:

$$\mathrm{ITS} \propto \int_{-\infty}^{+\infty} C(\tau)\mathrm{d}\tau \tag{B.2}$$

where C is the autocovariance. Note the integration limits. Davis then goes on to say that each ITS in a record corresponds to one DOF. Emery and Thomson (1998), on the other hand, have the following definition for the ITS, where again the notation has been simplified a little:

$$\mathrm{ITS} \propto \int_{0}^{+\infty} C(\tau)\mathrm{d}\tau. \tag{B.3}$$

Note again the integration limits. Emery and Thompson then also state that one ITS in a record corresponds to one DOF. Because the autocovariance function is symmetric with respect to zero lag, if one uses the ITS definition in Eq. (B.3) and one assumes that each ITS provides a DOF, one will find twice as many DOF as using the ITS definition in Eq. (B.2) for a record of the same length.

A review of the literature and discussions with many colleagues suggests that the ITS definition in Eq. (B.3) is the more commonly used one, however all sources seem to agree than the proper definition of the DOF is that given in Eq. (B.1). As such the proper relationship between ITS and DOF is that it requires two ITS calculated via Eq. (B.3) to provide one DOF. This is the result that shall be used in this paper. If instead one chooses to use the Eq. (B.2) definition of the ITS, one needs to associate one DOF with each ITS.

For the 12 bottom pressure records and the 24 travel time records from the PIES and IES the definition in Eq. (B.3) was applied. The mean (median) ITS for the pressure records was 20 (18) days, while the mean (median) ITS for the travel time records was 26 (27) days (n.b., ITS was calculated after the 40-h low-pass filtering). As the absolute velocities calculated as discussed herein are dependent on both the bottom pressure data and the travel time data, a mean ITS of 23 days is used throughout.

References

Bendat, J.S., Piersol, G., 1986. Random Data: Analysis and Measurement Procedures. Wiley-Interscience, New York, 566pp.

Bower, A.S., Hogg, N.G., 1996. Structure of the Gulf Stream and its recirculations at 55°W. Journal of Physical Oceanography 26 (6), 1002–1022.

Cronin, M., Watts, D.R., 1996. Eddy-mean flow interaction in the Gulf Stream at 68°W. Part I: Eddy energetics. Journal of Physical Oceanography 26 (10), 2107–2131.

Davis, R.E., 1976. Predictability of sea surface temperature and sea level pressure anomalies over the North Pacific Ocean. Journal of Physical Oceanography 6 (3), 249–266.

Davis, R.E., 1977. Techniques for statistical analysis and prediction of geophysical fluid systems. Geophysical and Astrophysical Fluid Dynamics 8, 245–277.

Del Grosso, V.A., 1974. New equation for the speed of sound in natural waters (with comparisons to other equations). Journal of the Acoustical Society of America 56, 1084–1091.

Emery, W.J., Thomson, R.E., 1998. Data Analysis Methods in Physical Oceanography. Elsevier, New York, 634pp.

Fofonoff, N.P., 1962. Dynamics of ocean currents. In: The Sea: Ideas and Observations on Progress in the Study of the Seas, vol. 1. Wiley-Interscience, New York, pp. 323–396 (Chapter 3).

Gill, A.E., 1982. Atmosphere-Ocean Dynamics. Academic Press, San Diego, 662pp.

Halkin, D., Rossby, T., 1985. The structure and transport of the Gulf Stream at 73°W. Journal of Physical Oceanography 15 (11), 1439–1452.

He, Y., Watts, D.R., Tracey, K.L., 1998. Determining geostrophic velocity shear profiles with inverted echo sounders. Journal of Geophysical Research 103 (C3), 5607–5622.

Hogg, N.G., 1992. On the transport of the Gulf Stream between Cape Hatteras and the Grand Banks. Deep-Sea Research 39, 1231–1246.

Hummon, J.M., Rossby, T., 1998. Spatial and temporal evolution of a Gulf Stream crest-warm core ring interaction. Journal of Geophysical Research 103 (C2), 2795–2809.

Johns, E., Watts, D.R., Rossby, H.T., 1989. A test of geostrophy in the Gulf Stream. Journal of Geophysical Research 94 (C3), 3211–3222.

Johns, W.E., Shay, T.J., Bane, J.M., Watts, D.R., 1995. Gulf Stream structure, transport, and recirculation near 68°W. Journal of Geophysical Research 100 (C1), 817–838.

Johns, W.E., Kanzow, T., Zantopp, R., 2005. Estimating ocean transports with dynamic height moorings: an application in the Atlantic deep western boundary current. Deep-Sea Research I 52 (8), 1542–1567.

Joyce, T.M., 1984. Velocity and hydrographic structure of a Gulf Stream warm-core ring. Journal of Physical Oceanography 14 (5), 936–947.

Joyce, T.M., Wunsch, C., Pierce, S.D., 1986. Synoptic Gulf Stream velocity profiles through simultaneous inversion of hydrographic

Author's personal copy

and acoustic Doppler data. Journal of Geophysical Research 91 (C6), 7573–7585.
Kim, H.-S., Watts, D.R., 1994. An observational streamfunction in the Gulf Stream. Journal of Physical Oceanography 24 (12), 2639–2657.
Leaman, K.D., Johns, E., Rossby, T., 1989. The average distribution of volume transport and potential vorticity with temperature at three sections across the Gulf Stream. Journal of Physical Oceanography 19 (1), 36–50.
Lee, T., Cornillon, P., 1996. Propagation of Gulf Stream meanders between 74° and 70°W. Journal of Physical Oceanography 26 (2), 205–224.
Lindstrom, S.S., Watts, D.R., 1994. Vertical motion in the Gulf Stream near 68°W. Journal of Physical Oceanography 24 (11), 2321–2333.
Lindstrom, S.S., Qian, X., Watts, D.R., 1997. Vertical motion in the Gulf Stream and its relation to meanders. Journal of Geophysical Research 102 (C4), 8485–8503.
Logoutov, O., Sutyrin, G., Watts, D.R., 2001. Potential vorticity structure across the Gulf Stream: observations and a PV-gradient model. Journal of Physical Oceanography 31 (2), 637–644.
Lozier, M.S., Owens, W.B., Curry, R.G., 1995. The climatology of the North Atlantic. Progress in Oceanography 36, 1–44.
Meinen, C.S., Luther, D.S., 2003. Comparison of methods of estimating mean synoptic current structure in "stream coordinates" reference frames with an example from the Antarctic Circumpolar Current. Deep-Sea Research I 50, 201–220.
Meinen, C.S., Watts, D.R., 1997. Further evidence that the sound speed algorithm of Del Grosso is more accurate than that of Chen and Millero. Journal of the Acoustical Society of America 102 (4), 2058–2062.
Meinen, C.S., Watts, D.R., 2000. Vertical structure and transport on a transect across the North Atlantic Current near 42°N: time series and mean. Journal of Geophysical Research 105 (C9), 21869–21891.
Meinen, C.S., Garzoli, S.L., Johns, W.E., Baringer, M.O., 2004. Transport variability of the deep western boundary current and the Antilles Current off Abaco Island, Bahamas. Deep-Sea Research I 51, 1397–1415.
Pickart, R.S., Watts, D.R., 1990a. Deep western boundary current variability at Cape Hatteras. Journal of Marine Research 48, 765–791.
Pickart, R.S., Watts, D.R., 1990b. Using the inverted echo sounder to measure vertical profiles of Gulf Stream temperature and geostrophic velocity. Journal of Atmospheric and Oceanic Technology 7 (2), 146–156.
Rossby, T., 1969. On monitoring depth variations of the main thermocline acoustically. Journal of Geophysical Research 74 (23), 5542–5546.
Rossby, T., Zhang, H.-M., 2001. The near-surface velocity and potential vorticity structure of the Gulf Stream. Journal of Marine Research 59, 949–975.
Sciremammano Jr., F., 1979. A suggestion for the presentation of correlations and their significance levels. Journal of Physical Oceanography 9 (11), 1273–1276.
Shay, T.J., Bane, J.M., Watts, D.R., Tracey, K.L., 1995. Gulf Stream flow field and events near 68°W. Journal of Geophysical Research 100 (C11), 22565–22589.
Smith, W.H.F., Sandwell, D.T., 1997. Global sea floor topography from satellite altimetry and ship depth soundings. Science 277 (5334), 1956–1962.
Tracey, K.L., Howden, S.D., Watts, D.R., 1997. IES calibration and mapping procedures. Journal of Atmospheric and Oceanic Technology 14 (6), 1483–1493.
Watts, D.R., Kontoyiannis, H., 1990. Deep-ocean bottom pressure measurement: drift removal and performance. Journal of Atmospheric and Oceanic Technology 7 (2), 296–306.
Watts, D.R., Rossby, H.T., 1977. Measuring dynamic heights with inverted echo sounders: results from MODE. Journal of Physical Oceanography 7, 345–358.
Watts, D.R., Tracey, K.L., Bane, J.M., Shay, T.J., 1995. Gulf Stream path and thermocline structure near 74°W and 68°W. Journal of Geophysical Research 100 (C9), 18291–18312.
Watts, D.R., Sun, C., Rintoul, S., 2001a. A two-dimensional gravest empirical mode determined from hydrographic observations in the subantarctic front. Journal of Physical Oceanography 31 (8), 2186–2209.
Watts, D.R., Qian, X., Tracey, K.L., 2001b. Mapping Abyssal current and pressure fields under the meandering Gulf Stream. Journal of Atmospheric and Oceanic Technology 18 (6), 1052–1067.
Worthington, L.V., 1959. The 18° water in the Sargasso Sea. Deep-Sea Research 5, 297–305.